

## Metalloenes

## How Hydrogen Bonds Affect Reactivity and Intervalence Charge Transfer in Ferrocenium-Phenolate Radicals

Andreas Neidlinger,<sup>[a]</sup> Christoph Förster,<sup>[a]</sup> and Katja Heinze\*<sup>[a]</sup>

**Abstract:** The ferrocenyl-phenol 2,4-di-*tert*-butyl-6-(ferrocenylcarbamoyl)phenol (**H-1**) forms intramolecular hydrogen bonds which are absent in its constitutional isomer 2,6-di-*tert*-butyl-4-(ferrocenylcarbamoyl)phenol (**H-2**). Their corresponding bases **1**<sup>-</sup> and **2**<sup>-</sup> show intra- and intermolecular NH...O hydrogen bonds, respectively. The phenolate **1**<sup>-</sup> is reversibly oxidized to **1**<sup>•</sup>, whereas **2**<sup>-</sup> only undergoes a quasi-reversible oxidation to **2**<sup>•</sup>, which suggests a higher reactivity. The radical pools of **1**<sup>•</sup> and **2**<sup>•</sup> formed by the oxidation/deprotonation of **H-1** and **H-2** have been probed by (rapid-freeze) electron paramagnetic resonance (EPR) spectroscopy and by spin-trapping techniques to elucidate the types of radicals present. Ferrocenium phenolate [**1a**]<sup>•</sup> featuring an NH...O intramolecular hydrogen bond is the most stable radical and undergoes thermal and photoinduced valence isomerization to the phenoxyl radical valence

isomer [**1b**]<sup>•</sup> with participation of the NH stretching mode (proton-coupled electron transfer). A ferrocenium iminolate radical [**1c**]<sup>•</sup> is present as well and equilibrates with the carbon-centered ferrocenyl radicals [**1c<sup>CP</sup>**]<sup>•</sup> and [**1b<sup>β</sup>**]<sup>•</sup>. The latter radicals are intercepted by nitrobenzene to give the corresponding stable nitroxyl radicals [**6c<sup>CP</sup>**]<sup>•</sup> and [**6b<sup>β</sup>**]<sup>•</sup>. All the radicals **2**<sup>•</sup>, which lack intramolecular hydrogen bonds, are transient in nature due to rapid follow-up reactions. However, rapid-freeze EPR spectroscopy indicated the presence of ferrocenium iminolate [**2c**]<sup>•</sup>, the phenoxyl radical [**2b**]<sup>•</sup>, and/or carbon-centered radicals [**2c<sup>CP</sup>**]<sup>•</sup> and [**2b<sup>β</sup>**]<sup>•</sup>. The carbon-centered radicals [**2c<sup>CP</sup>**]<sup>•</sup> and [**2b<sup>β</sup>**]<sup>•</sup> are selectively trapped as the corresponding nitroxide radicals [**7c<sup>CP</sup>**]<sup>•</sup> and [**7b<sup>β</sup>**]<sup>•</sup>. These diverse reactivity patterns are relevant for cytostatic ferrocenyl-phenols such as ferrocifen.

## Introduction

Electron-transfer (ET) reactions continue to be a focus of interest due to their importance in a plethora of chemical and biological processes.<sup>[1–7]</sup> Combination with proton-transfer (PT) reactions facilitates ET (proton-coupled electron transfer, PCET).<sup>[8–18]</sup> As a prominent example, in photosystem II, the tyrosyl residue (phenoxyl radical) is reduced to phenol(ate) by the oxygen-evolving complex through PCET with the assistance of a nearby histidine base as proton shuttle.<sup>[19–24]</sup> This PCET is a key process in the stepwise oxidation of the oxygen-evolving complex, which finally results in the oxidation of water to dioxygen at the oxygen-evolving complex, which is itself based on PCET processes.<sup>[19–24]</sup>

We have been interested in small model systems comprising a phenoxyl radical<sup>[25]</sup> and ferrocene<sup>[26–30]</sup> (and in the corresponding ferrocenium/phenolate valence isomers) to investigate PCET intervalence charge-transfer (IVCT)<sup>[31]</sup> reactions in redox-asymmetric systems.<sup>[16]</sup> In the parent ferrocenyl-phenol conjugate **H-1**,<sup>[16]</sup> an intramolecular hydrogen bond (IHB) is formed between the phenolic OH group and the carbonyl oxygen of the amide bond (OH...O IHB, Scheme 1, a), similarly to

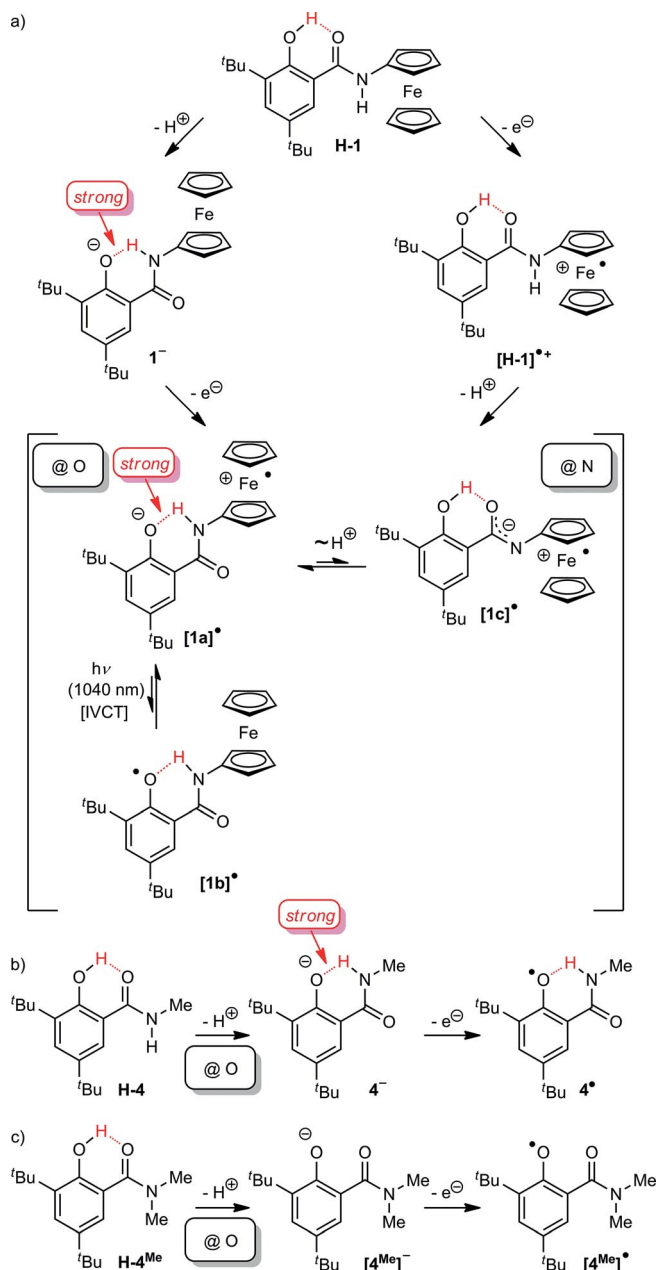
ferrocene-free salicylamide **H-4** (Scheme 1, b). The deprotonation and oxidation of **H-1** yields the ferrocenium phenolate zwitterion [**1a**]<sup>•</sup>; the valence isomeric ferrocenyl phenoxyl radical [**1b**]<sup>•</sup>; and the ferrocenium iminolate tautomer [**1c**]<sup>•</sup>. In the latter tautomer, the OH...O IHB is retained whereas an NH...O IHB is established in the valence isomers [**1a**]<sup>•</sup> and [**1b**]<sup>•</sup>.

The IHB of the zwitterion [**1a**]<sup>•</sup> is highly stabilized with respect to the IHB of the phenoxyl radical [**1b**]<sup>•</sup> for two reasons: First, the phenolate is a better hydrogen-atom acceptor than a phenoxyl radical, which is also observed for the IHB of the ferrocene-free reference phenolate/phenoxyl pair **4**<sup>-</sup> and **4**<sup>•</sup> (Scheme 1, b).<sup>[25]</sup> Secondly, the ferrocenium-amide is a stronger hydrogen-atom donor than the ferrocenyl-amide due to the positive charge. This phenomenon has been previously observed, for example, in oligoferrocene amides **H-A** and the corresponding mixed-valent systems [**H-A**]<sup>•+</sup> (Scheme 2, a).<sup>[28,29]</sup> Hence, the zwitterion [**1a**]<sup>•</sup> is considerably stabilized with respect to [**1b**]<sup>•</sup> (by 30 kJ mol<sup>-1</sup> according to DFT calculations).<sup>[16]</sup> The proton in the IHB is involved in the thermal intramolecular ET between [**1a**]<sup>•</sup> and [**1b**]<sup>•</sup>, with the proton being closer to the oxygen atom in [**1a**]<sup>•</sup> and closer to the nitrogen atom in [**1b**]<sup>•</sup>. Optical ET (IVCT absorption band at 1040 nm) from the ground state of [**1a**]<sup>•</sup> to give the metastable phenoxide [**1b**]<sup>•</sup> can only occur when the proton is already closer to the nitrogen atom, as found in [**1b**]<sup>•</sup>. Hence, the ET is coupled with the NH vibrational mode of the [**1a**]<sup>•</sup>/[**1b**]<sup>•</sup> valence isomers.

Charges stabilize the IHB and vice versa the hydrogen bond affects the redox potentials of the redox centers connected by

[a] Institute of Inorganic and Analytical Chemistry, Johannes Gutenberg University, Duesbergweg 10–14, 55128 Mainz, Germany  
E-mail: katja.heinze@uni-mainz.de  
<http://www.ak-heinze.chemie.uni-mainz.de/>

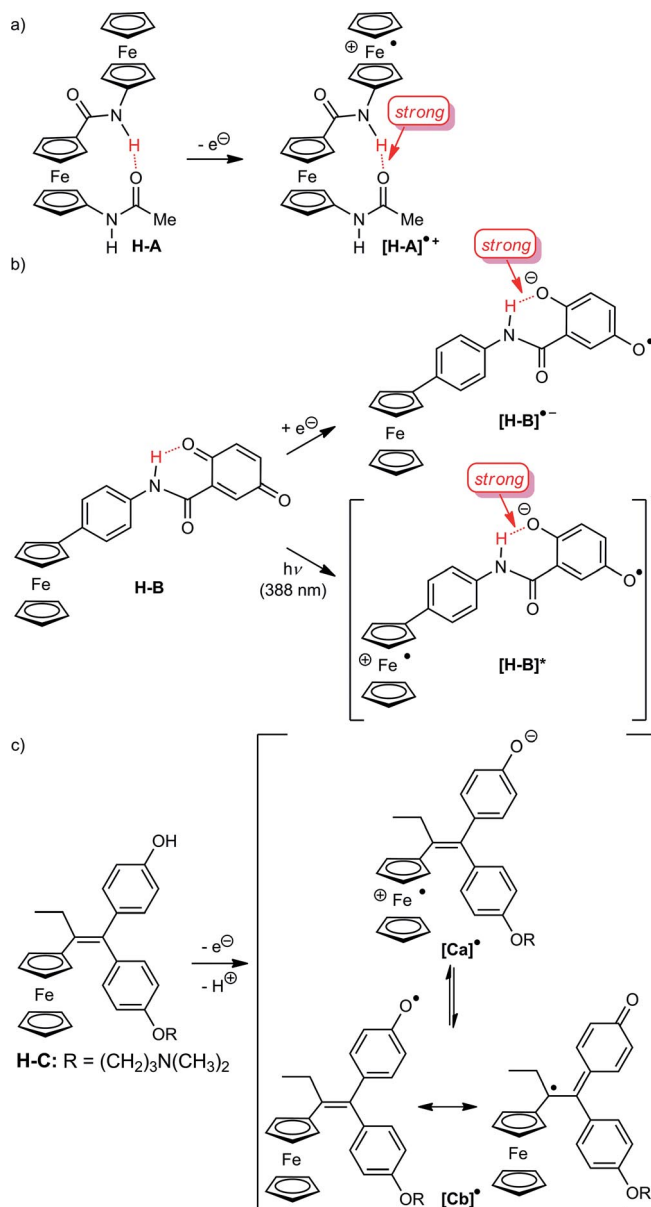
Supporting information for this article is available on the WWW under <http://dx.doi.org/10.1002/ejic.201501471>.



Scheme 1. Hydrogen bonding in salicyl amides **H-1**, **H-4**, and **H-4<sup>Me</sup>**, their corresponding phenolates **1<sup>-</sup>**, **4<sup>-</sup>**, and **[4<sup>Me</sup>]<sup>-</sup>**, and their corresponding phenoxyl radicals **1<sup>•</sup>**, **4<sup>•</sup>**, and **[4<sup>Me</sup>]<sup>•</sup>**.<sup>[16,25]</sup>

the IHB. Large potential differences are observed between hydrogen-bonded and non-hydrogen-bonded phenolate/phenoxyl couples such as **4<sup>-</sup>/4<sup>•</sup>** ( $E_{1/2} = -160$  mV vs. FcH/FcH<sup>+</sup> in CH<sub>3</sub>CN/[*n*Bu<sub>4</sub>N][BF<sub>4</sub>])<sup>[25]</sup> and **[4<sup>Me</sup>]<sup>-</sup>/[4<sup>Me</sup>]<sup>•</sup>** ( $E_{1/2} = -425$  mV vs. FcH/FcH<sup>+</sup> in CH<sub>3</sub>CN/[*n*Bu<sub>4</sub>N][BF<sub>4</sub>])<sup>[25]</sup> Scheme 1, b, c).<sup>[25]</sup> Similarly, the hydrogen-bonded ferrocenyl-NH moiety in **H-A** ( $E_{1/2} = -115$  mV vs. FcH/FcH<sup>+</sup> in CH<sub>3</sub>CN/[*n*Bu<sub>4</sub>N][PF<sub>6</sub>])<sup>[27,28]</sup> is oxidized at a lower potential than *N*-acetylferrocene **H-3** ( $E_{1/2} = -50$  mV vs. FcH/FcH<sup>+</sup> in CH<sub>2</sub>Cl<sub>2</sub>/[*n*Bu<sub>4</sub>N][B(C<sub>6</sub>F<sub>5</sub>)<sub>4</sub>])<sup>[26,27,29,30]</sup> Scheme 2, a).

Another intriguing example of this kind of PCET with the crucial NH...O IHB is found for the amide-linked ferrocenyl-quin-

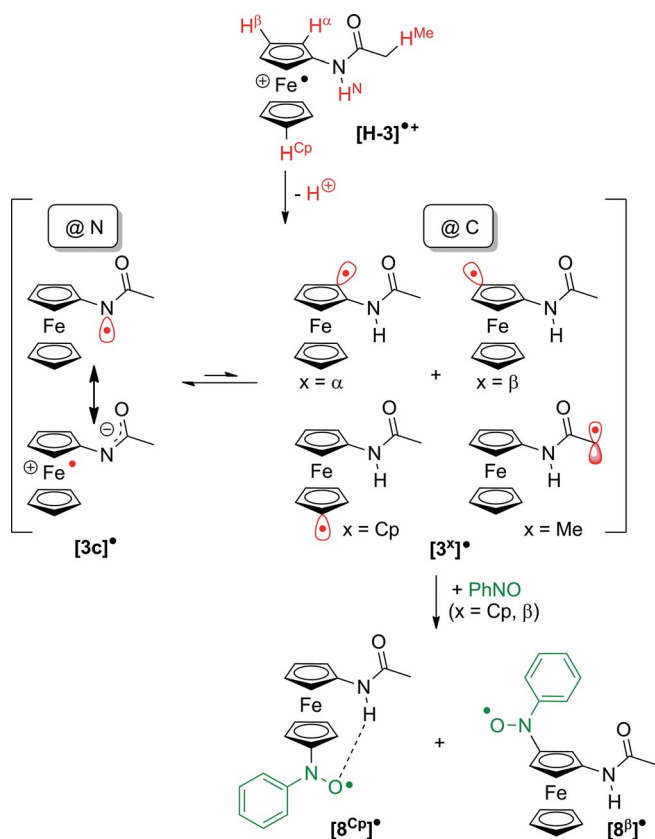


Scheme 2. a,b) IHBs in the ferrocene/ferrocenium amide redox couples **H-A**/**[H-A]<sup>•+</sup>** and **H-B**/**[H-B]<sup>•-</sup>** and c) ET and PT from the ferrocenyl-phenol ferrocifen (**H-C**).

one dyad **H-B** (Scheme 2, b).<sup>[32]</sup> Upon reduction of the quinone to the semiquinonate **[H-B]<sup>•-</sup>**, the NH...O IHB is strengthened and the semiquinone radical anion is stabilized. Similarly, the irradiation of **H-B** at 388 nm yields the charge-separated state **[H-B]\*** with ferrocenium-semiquinonate character effecting a strong NH...O IHB. Owing to the stabilizing effect of this IHB, the lifetime of this zwitterionic state **[H-B]\*** is quite high (Scheme 2, b).<sup>[32]</sup>

Ferrocenyl-phenols such as ferrocifen (**H-C**; Scheme 2, c) have attracted considerable interest as potent anticancer drugs.<sup>[33]</sup> Indeed, oxidation and deprotonation yields the mesomeric phenoxyl radical/C-centered radical **[Cb]<sup>•</sup>** and the conceivable ferrocenium phenolate zwitterionic valence isomer **[Ca]<sup>•+</sup>**, both lacking IHBs.

In this context, we recently succeeded in capturing transient carbon-centered ferrocenyl radicals, as proposed for **[Cb]**, by using nitrosobenzene (PhNO) as spin trap.<sup>[26]</sup> Relevant to the present study is the formation of trace amounts of C-centered radicals **[3<sup>x</sup>]** derived from *N*-acetylferrocene (**H-3**) in the presence of a base and an oxidant, in addition to the more stable ferrocenium iminolate radical **[3c]** (Scheme 3). The EPR spectra of the nitroxyl radicals **[8<sup>x</sup>]** resulting from the trapping of C-centered radicals **[3<sup>x</sup>]** by PhNO revealed the preferred site of attack, namely on the unsubstituted cyclopentadienyl ring and the  $\beta$  position with respect to the acetyl amino group (**[8<sup>Cp</sup>]**, **[8 <sup>$\beta$</sup> ]**; Scheme 3).<sup>[26]</sup> The ferrocenium iminolate **[3c]** does not react with PhNO, neither at the nitrogen atom nor at the metal center.<sup>[26]</sup>



Scheme 3. Radical reactivity of **[H-3]<sup>+</sup>** in the presence of a base and PhNO.<sup>[26]</sup>

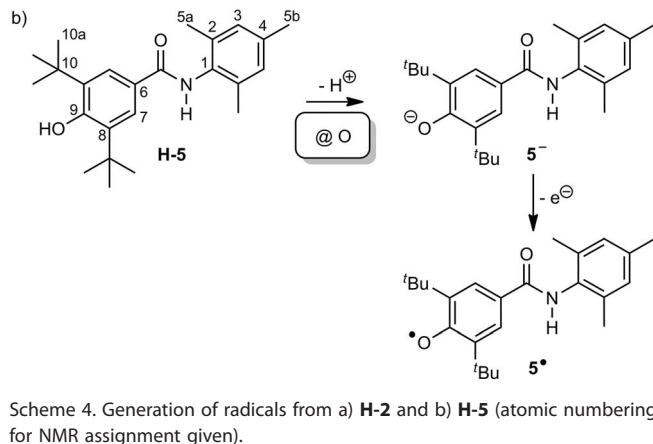
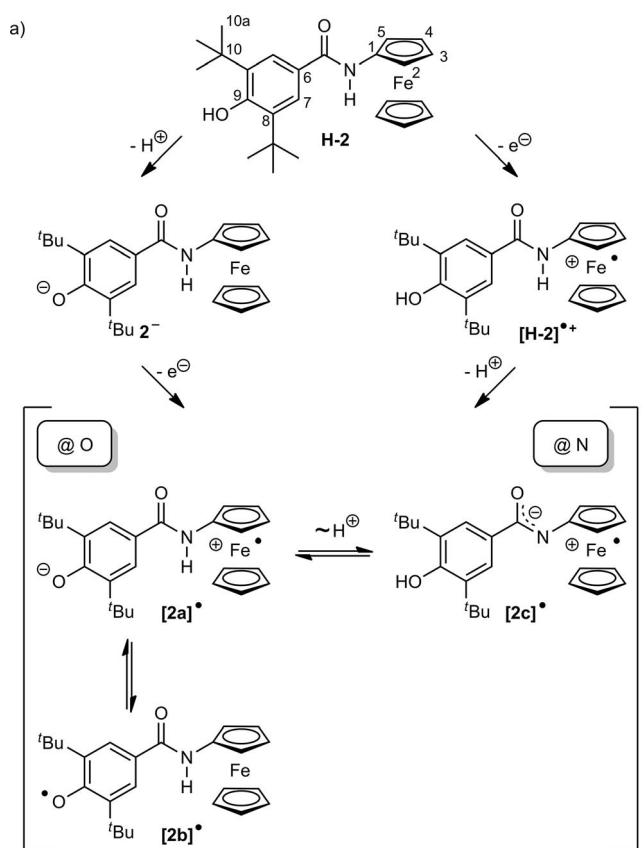
In this study we addressed the effect of the NH...O IHB in **1** on the reactivity and distribution of valence isomers (ferrocenium phenolate zwitterion **[1a]** vs. phenoxyl radical **[1b]**) and tautomers (ferrocenium iminolate **[1c]**; C-centered radicals **[1<sup>x</sup>]**). To eliminate all the IHBs while essentially maintaining the overall geometry and electronic structure, the phenolic OH group is formally shifted from the 2-position in **H-1** to the 4-position in the constitutional isomer **H-2** (Scheme 4). The properties of phenol **H-2**, its conjugate base **2<sup>-</sup>**, its oxidation product **[H-2]<sup>+</sup>**, and the conceivable radical species **[2a]**, **[2b]**, **[2c]**, and **[2<sup>x</sup>]** were studied by (rapid-freeze) EPR spectroscopy and DFT calculations and contrasted with the corresponding species derived from **H-1**. The potential presence of the C-centered radicals **[1<sup>x</sup>]** and **[2<sup>x</sup>]** (in analogy to **[3<sup>x</sup>]**) derived from the

corresponding ferrocenyl-phenols **H-1** and **H-2** in the presence of base and oxidant was probed by the spin-trapping technique. The possible presence of different radical types is relevant for the reactivity of cytostatic drugs based on the ferrocenyl-phenol motif, such as ferrocifen (**H-C**).

## Results and Discussion

### Synthesis and Characterization of Ferrocenyl Phenols **H-1** and **H-2** and Reference Phenols **H-4** and **H-5**

The phenols **H-1** and **H-4** were prepared according to literature procedures<sup>[16,25]</sup> (Scheme 1). The constitutional isomer of **H-1**, 2,6-di-*tert*-butyl-4-(ferrocenylcarbamoyl)phenol (**H-2**; Scheme 4, a), was obtained by condensation of aminoferrocene<sup>[27]</sup> with the commercially available benzoic acid derivative 3,5-di-*tert*-



Scheme 4. Generation of radicals from a) **H-2** and b) **H-5** (atomic numbering for NMR assignment given).

butyl-4-hydroxybenzoic acid with HATU (1-[bis(dimethylamino)-methylene]-1*H*-1,2,3-triazolo[4,5-*b*]pyridinium 3-oxide hexafluorophosphate) as coupling reagent. The ferrocene-free reference phenol **H-5** [2,6-di-*tert*-butyl-4-(2,4,6-trimethylphenyl-carbamoyl)phenol, Scheme 4, b] was accessible by an analogous coupling of the same benzoic acid derivative with 2,4,6-trimethylaniline. Both phenols were fully characterized by NMR and IR spectroscopy as well as by mass spectrometry and elemental analysis.

The molecular ion peak of **H-2** is at  $m/z = 433$  in the FD mass spectrum. The  $^1\text{H}$  NMR spectrum of **H-2** displays the expected number of resonances with correct integral ratios. Owing to the low solubility of **H-2** in dichloromethane, more detailed NMR studies ( $^{13}\text{C}$  NMR, 2D NMR) were also conducted in  $[\text{D}_8]\text{THF}$ . In this coordinating solvent, the NH and OH protons resonate at  $\delta_{\text{NH}} = 8.50$  ppm and  $\delta_{\text{OH}} = 6.59$  ppm, respectively. These two resonances were unambiguously assigned by NOE spectroscopy (see Figure S1a in the Supporting Information). Contacts between the NH proton and the  $\alpha$ -ferrocenyl protons 2,5-H ( $\delta = 4.71$  ppm) as well as the aromatic protons 7-H ( $\delta = 7.73$  ppm) are observed (Scheme 4). As expected, the OH proton shows a contact with the *t*Bu groups ( $\delta = 1.47$  ppm). These chemical shifts suggest the absence of hydrogen bonds in **H-2**, in contrast to its constitutional isomer **H-1**, which features an OH...O IHB ( $\delta_{\text{NH}} = 9.01$  ppm,  $\delta_{\text{OH}} = 13.37$  ppm in  $[\text{D}_8]\text{THF}$ ; Scheme 1).<sup>[16,35]</sup> Similarly, in  $\text{CD}_2\text{Cl}_2$ , the resonances for the NH and OH protons are found at  $\delta_{\text{NH}} = 7.09$  and 7.36 ppm and  $\delta_{\text{OH}} = 5.63$  and 12.69 ppm for **H-2** and **H-1**, respectively. Hence, weak intermolecular hydrogen bonds from NH/OH to THF are likely, but IHBs of any kind are clearly absent in **H-2**.

The IR spectrum of **H-2** in  $\text{CH}_2\text{Cl}_2$  confirms the absence of IHBs involving NH or OH groups. The absorption for the NH stretching vibration is observed at  $\tilde{\nu}_{\text{NH}} = 3440\text{ cm}^{-1}$ , similarly to those of **H-3** ( $\tilde{\nu}_{\text{NH}} = 3435\text{ cm}^{-1}$ )<sup>[27]</sup> and **H-1** ( $\tilde{\nu}_{\text{NH}} = 3450\text{ cm}^{-1}$ )<sup>[16]</sup> characteristic of a free NH group. The free OH group of **H-2** shows an absorption at  $\tilde{\nu}_{\text{OH}} = 3625\text{ cm}^{-1}$ . In contrast, the OH stretching vibration of **H-1** is not observed in the spectral region between  $3800\text{--}3100\text{ cm}^{-1}$  due to its involvement in the OH...O IHB (Scheme 1).<sup>[16]</sup>

The reference phenol **H-5** was similarly characterized (see the Exp. Sect. and Figure S1b in the Supporting Information). As expected, no IHBs were detected for **H-5** in  $\text{CDCl}_3$  by  $^1\text{H}$  NMR spectroscopy ( $\delta_{\text{OH}} = 5.60$  ppm and  $\delta_{\text{NH}} = 7.18$  ppm) or in  $\text{CH}_2\text{Cl}_2$  by IR spectroscopy ( $\tilde{\nu}_{\text{OH}} = 3625\text{ cm}^{-1}$  and  $\tilde{\nu}_{\text{NH}} = 3425\text{ cm}^{-1}$ ).

The presence of the OH...O IHB in **H-1**, as suggested by NMR and IR studies in solution,<sup>[16]</sup> was further corroborated by single-crystal XRD analysis. **H-1** crystallizes from ethyl acetate at 4 °C in the monoclinic space group  $P2_1/c$  (Figure 1). The ferrocenyl moiety shows the usual structural features. The OH...O IHB has an O1...O2 distance of 2.580(3) Å. Furthermore, intermolecular hydrogen bonds between the amide proton and the carbonyl oxygen O1' of neighboring molecules of **H-1** lead to the typical hydrogen-bonded chain of amides in the solid state with an N1...O1' distance of 3.220(3) Å.<sup>[27,28]</sup> Additional crystallographic details are given in the Table S1 and Figure S2 in the Supporting Information.

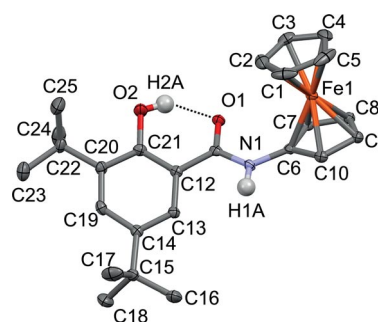


Figure 1. Molecular structure of **H-1** in the solid state. Thermal ellipsoids are drawn at the 50% probability level. CH hydrogen atoms have been omitted for clarity.

### Radical Formation and Radical Characterization

The PT and ET reactions of **H-1/H-2** and their corresponding reference phenols **H-4/H-5** are depicted in Schemes 1 and 4. The chemical oxidations were performed by using silver hexafluoroantimonate ( $\text{AgSbF}_6$ ) as oxidant [ $E_{1/2}(\text{CH}_2\text{Cl}_2) = 650\text{ mV}$  vs.  $\text{FcH}/\text{FcH}^+$ ]<sup>[36]</sup> which is capable of oxidizing the ferrocenyl as well as the phenolate unit. Deprotonation was achieved by using the non-nucleophilic and non-coordinating phosphazene base  $\text{P}_1\text{tBu}$  [*tert*-butyliminotris(dimethylamino)phosphorane,  $\text{p}K_a(\text{MeCN}) = 26.98$ ]<sup>[37]</sup> as proton acceptor. All analyses, oxidations, and deprotonations were performed under an inert atmosphere. After filtration of precipitated silver when applicable, the resulting solutions were immediately subjected to spectroscopic analyses (IR, UV/Vis, and EPR spectroscopy).

The reference radical **4** obtained from **H-4** by PT and ET gives the expected sharp EPR resonance of a phenoxyl radical at  $g_{1,2,3} = 2.0117, 2.0071, 2.0037$  (Table 2) at 77 K and at  $g_{\text{iso}} =$

Table 1. EPR parameters obtained by simulation of the experimental X-band EPR spectra recorded at 298 K.<sup>[a]</sup>

Radical	$g_{\text{iso}}$	$A(^{14}\text{N})$ [G]	$A(^1\text{H}^o)$ [G]	$A(^1\text{H}^m)$ [G]	$A(^1\text{H}^p)$ [G]	Other $A(^1\text{H})$ [G]	Gauss pp linewidth [MHz]	Lorentz pp linewidth [MHz]
<b>[1b]</b>	2.0059						0.4	0.4
<b>4</b>	2.0058					1.8/0.95 <sup>[b]</sup>	0.1	0.07
<b>5</b>	2.0060	1.90 <sup>[c]</sup>				1.7 (2 $\times$ ) <sup>[d]</sup>	0.02	0.02
<b>[6<sup>CP</sup>]</b>	2.0071	11.10	2.80 (2 $\times$ )	0.90 (2 $\times$ )	2.60	1.20, 1.00, 0.90 (2 $\times$ ) <sup>[e]</sup>	0.08	0.04
<b>[7<sup>CP</sup>]</b>	2.0069	11.30	2.90 (2 $\times$ )	0.85 (2 $\times$ )	2.70	1.10 (2 $\times$ ), 0.85 (2 $\times$ ) <sup>[e]</sup>	0.15	0.05
<b>[8<sup>CP</sup>]</b> <sup>[f]</sup>	2.0072	10.90	2.77 (2 $\times$ )	0.90 (2 $\times$ )	2.64	1.20/1.10, 0.70 (2 $\times$ ) <sup>[e]</sup>	0.06	0.02

[a] For atomic numbering of the nitroxyl radicals, see Scheme 7. [b] Hydrogen atoms of the 3,5-di-*tert*-butyl-2-hydroxybenzoic acid moiety. [c] Amide nitrogen atom. [d] Hydrogen atoms of the 2,6-di-*tert*-butyl-4-hydroxybenzoic acid moiety. [e] Hydrogen atoms of the ferrocenyl moiety. [f] See ref.<sup>[26]</sup>

2.0058 at 298 K in  $\text{CH}_2\text{Cl}_2$  (Figure 2, Table 1).<sup>[16]</sup> The most stable valence isomer of **1'**, obtained by oxidation and deprotonation of **H-1**, is the zwitterionic **[1a]'**. The zwitterion is characterized by its 77 K EPR resonance ( $g_{1,2,3} = 3.0400, 1.9490, 1.9030$ ; Table 2), which significantly differs from the EPR pattern of the parent ferrocenium ion **[H-1]'+** ( $g_{1,2,3} = 3.4200, 1.8552, 1.7550$ ; Table 2).<sup>[16]</sup> Attempts to observe the expected trace amounts of the phenoxyl radical valence isomer **[1b]'** were recently successful and it shows a very weak EPR resonance at  $g_{\text{iso}} = 2.0059$  at 298 K (Figure 2, Table 1). At this temperature, the resonance of the ferrocenium-phenolate **[1a]'** is not observed. This is typical for ferrocenium radicals as these are EPR-silent at room temperature due to fast spin-lattice relaxation.<sup>[38]</sup> The signal of **[1b]'** is broader than that of **4'**, possibly due to additional unresolved

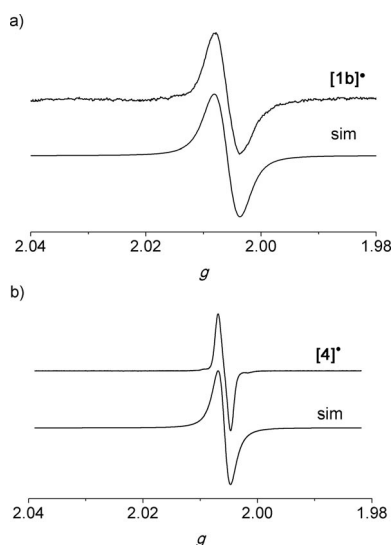


Figure 2. a) X-band EPR spectrum of **[1b]'** (20 mM solution of **H-1** in  $\text{CH}_2\text{Cl}_2$ ) at 298 K, including a simulation obtained by using the following parameters: field: 3346.20 G, sweep: 499.77 G, sweep time: 90 s, modulation: 5000 mG, MW attenuation: 10 dB. b) X-band EPR spectrum of **4'** (5 mM solution of **H-4** in  $\text{CH}_2\text{Cl}_2$ ) at 298 K, including a simulation obtained by using the following parameters: field: 3346.20 G, sweep: 94.79 G, sweep time: 90 s, modulation: 1000 mG, MW attenuation: 10 dB.<sup>[16]</sup>

hyperfine coupling (hfc) constants to ferrocenyl protons (Figure 2). The yield of **[1b]'** with respect to the initial **H-1**, obtained by double integration of the EPR resonance referenced against the 2,2-diphenyl-1-picrylhydrazyl (DPPH) radical, was approximately 0.05 %.<sup>[26,39]</sup> This low yield explains the difficulty of its observation.

We also attempted to detect the conceivable IVCT band of **[1b]'** in addition to the IVCT band of **[1a]'** (1040 nm in  $\text{CH}_2\text{Cl}_2$ ),<sup>[16]</sup> even though **[1b]'** is only present in trace amounts. Indeed, by close inspection of the NIR spectral region we were able to observe two further very weak NIR bands at 1970 and 1820 nm ( $\tilde{\nu}_{\text{max}} = 5076$  and  $5491 \text{ cm}^{-1}$ ,  $\Delta\tilde{\nu}_{1/2} = 548$  and  $815 \text{ cm}^{-1}$ ,  $\epsilon = 45$  and  $27 \text{ M}^{-1} \text{ cm}^{-1}$ ) in  $\text{CH}_2\text{Cl}_2$  (obtained by Gaussian deconvolution; see Figure S3 in the Supporting Information). However, the width,  $\Delta\tilde{\nu}_{1/2}$ , of these bands is rather low and smaller than expected for IVCT transitions.<sup>[40]</sup> These two low-energy bands are fairly similar to those observed for NHR-substituted ferrocenium ions such as **[H-3]'+**<sup>[41a]</sup> and other substituted  $\text{Fc}^+$  ions<sup>[41b]</sup> and have been attributed to Laporte-forbidden d–d transitions of the ferrocenium moiety. To further confirm this assignment, a time-dependent density functional theory (TD-DFT) calculation [B3LYP/SV(P), COSMO  $\text{CH}_2\text{Cl}_2$ ] was performed for **[1a]'**, which provided low-energy transitions at 2765, 2055, 1317, 1091, 997, and 771 nm (3617, 4865, 7594, 9168, 10031, and  $12973 \text{ cm}^{-1}$ , respectively; see Table S2 in the Supporting Information). The calculated lowest-energy band corresponds to an IVCT [phenolate  $\rightarrow d_{xy}(\text{Fc}^+)$ ,  $f = 0.00623$ ] giving the ferrocenyl phenoxyl radical ground state of **[1b]'**. This band was not observed experimentally. The 1091 nm band [phenolate  $\rightarrow d_{xz}(\text{Fc}^+)$ ,  $f = 0.01999$ ] corresponds to the experimentally observed IVCT band of **[1a]'** (1040 nm).<sup>[16]</sup> The calculated transitions at 2055 and 1317 nm have been assigned to the experimentally observed weak NIR bands at 1970 and 1820 nm and are clearly ferrocenium d–d transitions (see Table S2 and Figure S4 in the Supporting Information). Two further IVCT bands were calculated by TD-DFT at 997 and 771 nm ( $10031$  and  $12973 \text{ cm}^{-1}$ ). These represent phenolate  $\rightarrow d_{yz}(\text{Fc}^+)$  and lone pair (phenolate)  $\rightarrow d_{xy}(\text{Fc}^+)$  transitions. As they are close to the 1040 nm IVCT band and very weak in

Table 2. EPR parameters obtained by simulation of experimental X-band spectra recorded at 77 K.

Radical (mixture)	$g_{1,2,3}$	$A(^{14}\text{N})$ [G] (nitroxyl N)	Fraction [%]	Gauss pp linewidth [MHz]	Lorentz pp linewidth [MHz]
<b>[H-1]'+</b> <sup>[a]</sup>	3.4200, 1.8552, 1.7550			1.5	1.5
<b>[1a]'</b> <sup>[a]</sup>	3.0400, 1.9490, 1.9030			0.5	0.5
<b>[H-2]'+</b>	3.4000, 1.8780, 1.7965			1.0	1.0
<b>[H-3]'+</b> <sup>[a]</sup>	3.3500, 1.8750, 1.7870			1.5	1.5
<b>[1<math>\alpha</math>]'</b> ( $x = \alpha, \beta, \text{Cp}$ )	2.0105, 2.0070, 2.0025		1.3	0.5	0.5
<b>[1c]'</b>	2.9600, 1.9530, 1.9330		98.7	0.5	0.5
<b>[2b]'/[2<math>\alpha</math>]'</b> ( $x = \alpha, \beta, \text{Cp}$ )	$\approx 2.011, 2.008, 2.005$		30	0.3	0.3
<b>[2c]'</b>	N/A, $\approx 1.98, \approx 1.96$		70	1.7	1.7
<b>[8<math>\text{Cp}</math>]'</b> <sup>[b]</sup>	2.0105, 2.0060, 2.0045	3.5, 3.5, 28.0	17	0.3	0.4
<b>[3c]'</b> <sup>[b]</sup>	N/A, 1.9620, 1.9450		83	0.3	0.2
<b>[3<math>\alpha</math>]'</b> ( $x = \alpha, \beta, \text{Cp, Me}$ ) <sup>[b]</sup>	2.0095, 2.0065, 2.0030		0.8	0.3	0.2
<b>[3c]'</b> <sup>[26]</sup>	N/A, 1.9650, 1.9400		99.2	0.1	0.1
<b>4'</b>	2.0117, 2.0071, 2.0037			0.6	0.5
<b>5'</b>	2.0096, 2.0065, 2.0036			0.3	0.3
<b>[6<math>\text{Cp}</math>]'</b>	2.0103, 2.0069, 2.0040	3.0, 3.0, 28.0		0.5	0.5
<b>[7<math>\text{Cp}</math>]'</b>	2.0094, 2.0067, 2.0048	4.0, 4.0, 26.0		0.5	0.6

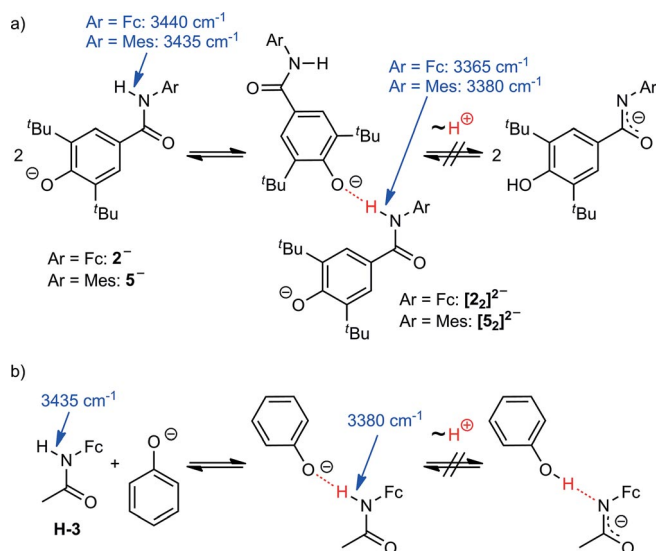
[a] See ref.<sup>[16]</sup> [b] See ref.<sup>[26]</sup>

intensity ( $f < 0.0001$ ) they are not distinctly observed. In essence, the relevant bands of **[1a]**<sup>−</sup> are well understood, whereas the IVCT bands of **[1b]**<sup>−</sup> are not detectable due to its very low concentration. Clearly, **[1a]**<sup>−</sup> is significantly preferred over **[1b]**<sup>−</sup> due to the strong NH...O IHB in the zwitterion.

The phenol amides **H-1** and **H-4** were easily deprotonated by using 1 equivalent of P<sub>1</sub>tBu in CH<sub>2</sub>Cl<sub>2</sub>. The analogous reaction with the constitutional isomers **H-2** and **H-5** proved to be more challenging, based on the results of UV/Vis and IR spectroscopic studies, namely an incomplete shift of the  $\pi$ - $\pi^*$  phenol/phenolate band<sup>[42,43]</sup> and an incomplete decrease of the  $\tilde{\nu}_{\text{OH}} = 3625 \text{ cm}^{-1}$  IR absorption band (see Figures S6a–S9a in the Supporting Information). Increasing the ionic strength of the CH<sub>2</sub>Cl<sub>2</sub> solution by the addition of [nBu<sub>4</sub>N][B(C<sub>6</sub>F<sub>5</sub>)<sub>4</sub>] (similar to the electrochemical experiments<sup>[44,45]</sup> see below) resulted in the almost complete deprotonation of **H-5** to **5**<sup>−</sup> and the quantitative deprotonation of **H-2** to **2**<sup>−</sup> by using 1 equivalent of P<sub>1</sub>tBu, based on the  $\pi$ - $\pi^*$  phenolate bands and the absence of OH vibrational stretching bands (see Figures S6b–S9b in the Supporting Information). Clearly, proton transfer benefits from a higher ionic strength of the solution.

The NH stretching vibrational bands of **2**<sup>−</sup> and **5**<sup>−</sup> ( $\tilde{\nu}_{\text{NH}} = 3435 \text{ cm}^{-1}$ ) are essentially unperturbed in comparison with those of **H-2** and **H-5** (see Figures S7b and S9b in the Supporting Information). However, an additional NH stretching band is found at  $\tilde{\nu}_{\text{NH}} = 3365$  and  $3380 \text{ cm}^{-1}$  for **2**<sup>−</sup> and **5**<sup>−</sup>, respectively. These bands have been assigned to an NH group intermolecularly hydrogen bonded to a phenolate ion to give at least dimeric aggregates **[2<sub>2</sub>]<sup>2−</sup>** and **[5<sub>2</sub>]<sup>2−</sup>** in CH<sub>2</sub>Cl<sub>2</sub> solution (Scheme 5, a; intermolecular NH...O hydrogen bond). Higher aggregates of these ionic systems **2**<sup>−</sup> and **5**<sup>−</sup> might also be present, but these are not shown for clarity. The presence of intermolecular hydrogen bonds is supported by the analogous association of **H-3** and phenolate (Scheme 5, b and Figure S10 in the Supporting Information;  $\tilde{\nu}_{\text{NH}} = 3380 \text{ cm}^{-1}$ ). As expected from the different pK<sub>a</sub> values of phenol and amide<sup>[35,46]</sup> and corroborated by DFT calculations, with the phenolate favored over the iminolate by 65 and 71 kJ mol<sup>−1</sup> for **2**<sup>−</sup> and **5**<sup>−</sup>, respectively (see Figure S11 in the Supporting Information), no evidence for the presence of conceivable iminolate tautomers is found (Scheme 5). That the NH group of amide **2**<sup>−</sup> should be sterically accessible for hydrogen bonding is also evident from the solid-state structure of **H-1** and other substituted *N*-ferrocenyl amides (see Figure S2 in the Supporting Information). The intermolecular NH...O hydrogen bond observed between the amide and phenolate is electronically congruent with the intramolecular NH...O hydrogen bond in **1**<sup>−</sup> (Scheme 1;  $\tilde{\nu}_{\text{NH}} = 3380 \text{ cm}^{-1}$ ).<sup>[16]</sup>

**H-2** was reversibly oxidized to **[H-2]<sup>+</sup>** at  $E_{1/2} = -105 \text{ mV}$  versus FcH/FcH<sup>+</sup> at 298 K in CH<sub>2</sub>Cl<sub>2</sub>/[nBu<sub>4</sub>N][B(C<sub>6</sub>F<sub>5</sub>)<sub>4</sub>] solution (see Figure S12 in the Supporting Information). Under the same conditions, the **H-1**/[**H-1**]<sup>+</sup> redox couple was observed at  $E_{1/2} = -150 \text{ mV}$ .<sup>[16]</sup> The EPR spectrum of **[H-2]<sup>+</sup>** in frozen CH<sub>2</sub>Cl<sub>2</sub>/[nBu<sub>4</sub>N][B(C<sub>6</sub>F<sub>5</sub>)<sub>4</sub>] at 77 K, obtained by the oxidation of **H-2** with AgSbF<sub>6</sub>, shows a characteristic, nearly axial ferrocenium resonance (see Figure S13 in the Supporting Information), similar to that of the ferrocenium ion **[H-1]<sup>+</sup>**,<sup>[16]</sup> thereby fully confirming



Scheme 5. a) Formation of **[2<sub>2</sub>]<sup>2−</sup>** and **[5<sub>2</sub>]<sup>2−</sup>** from **2**<sup>−</sup> and **5**<sup>−</sup> through intermolecular hydrogen bonds and b) intermolecular hydrogen bond between **H-3** and phenolate in CH<sub>2</sub>Cl<sub>2</sub> solution.

the metal-centered oxidation (Table 2). The UV/Vis spectrum of **[H-2]<sup>+</sup>**, prepared under the same conditions, features the expected ferrocenium absorption band at  $\lambda_{\text{max}} = 770 \text{ nm}$  (see Figure S14 in the Supporting Information), similarly to **[H-1]<sup>+</sup>**.<sup>[16,28,29]</sup> The IR spectrum of **[H-2]<sup>+</sup>**, prepared in the same fashion, shows an essentially unperturbed OH vibration ( $\tilde{\nu}_{\text{OH}} = 3620 \text{ cm}^{-1}$ ) and a slightly shifted NH vibration ( $\tilde{\nu}_{\text{NH}} = 3365 \text{ cm}^{-1}$ ). This suggests a weakening of the NH bond in the cation **[H-2]<sup>+</sup>** and hence an acidification of the NH group due to the positive charge on the ferrocenium moiety close to the NH group, which results in coordination of the counter ion to the NH group [NH...F(SbF<sub>6</sub>)].<sup>[16]</sup>

In the presence of approximately equimolar amounts of P<sub>1</sub>tBu, **H-2**, that is, phenolate **2**<sup>−</sup>, shows several distinct redox processes in CH<sub>2</sub>Cl<sub>2</sub>/[nBu<sub>4</sub>N][B(C<sub>6</sub>F<sub>5</sub>)<sub>4</sub>] solution. An irreversible oxidation at  $E_p = -500 \text{ mV}$  versus FcH/FcH<sup>+</sup> is observed followed by a reversible, one-electron oxidation process at  $E_{1/2} = -110 \text{ mV}$  versus FcH/FcH<sup>+</sup> and another irreversible follow-up wave at  $E_p = 70 \text{ mV}$  (Figure 3, bottom). The potential of the reversible wave ( $E_{1/2} = -110 \text{ mV}$ ) is close to that of the **H-2**/[**H-2**]<sup>+</sup> pair and the irreversible wave resembles that of the **5**<sup>−</sup>/**5**<sup>•−</sup>

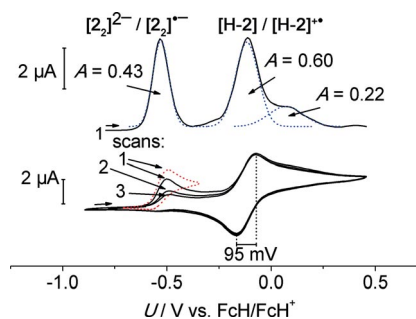
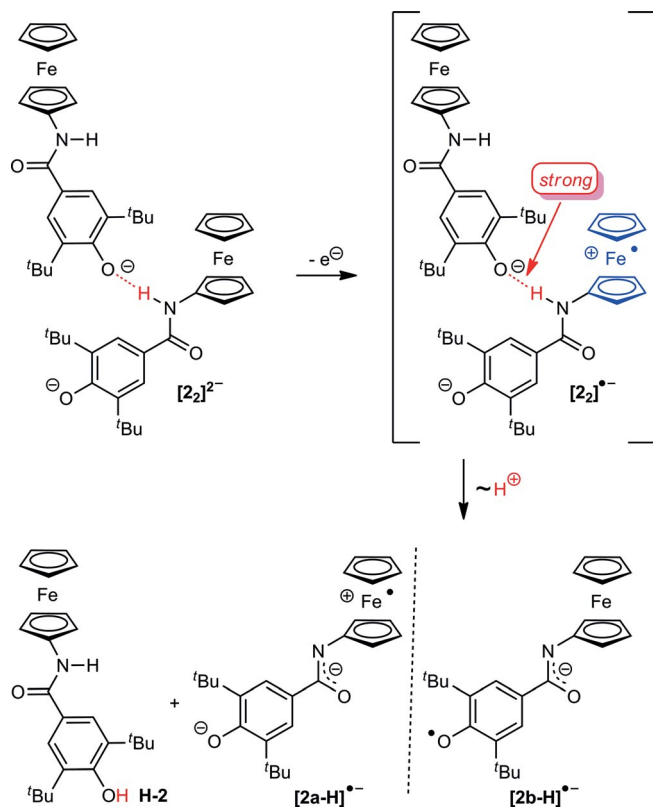


Figure 3. Square-wave (top) and cyclic voltammograms (bottom) of **2**<sup>−</sup> in CH<sub>2</sub>Cl<sub>2</sub> containing [nBu<sub>4</sub>N][B(C<sub>6</sub>F<sub>5</sub>)<sub>4</sub>] as supporting electrolyte at 298 K. Relative peak areas A are given.

reference couple ( $E_{1/2} = -490$  mV vs. FcH/FcH<sup>+</sup>; see Figure S15b in the Supporting Information). The reversible wave has indeed been assigned to the **H-2**/[**H-2**]<sup>+</sup> pair. As both **5**<sup>-</sup> and **2**<sup>-</sup> are present as (at least dimeric) aggregates (Scheme 5), we assigned the first wave to the irreversible oxidation of the hydrogen-bonded aggregate [**2**<sub>2</sub>]<sup>2-</sup> to the hydrogen-bonded radical [**2**<sub>2</sub>]<sup>•-</sup>. At higher scan rates (up to 800 mV s<sup>-1</sup>), the irreversible oxidation of [**2**<sub>2</sub>]<sup>2-</sup> becomes partially reversible (see Figure S16 in the Supporting Information). The fact that the peak area of the two high potential waves is approximately twice that of the area of the [**2**<sub>2</sub>]<sup>2-</sup>/[**2**<sub>2</sub>]<sup>•-</sup> oxidation wave (Figure 3, top) suggests that the oxidation of [**2**<sub>2</sub>]<sup>2-</sup> releases the phenol **H-2** after proton transfer and another species (Scheme 6). Furthermore, the wave of the initially present aggregated phenolate [**2**<sub>2</sub>]<sup>2-</sup> decreases upon further scanning, which confirms a follow-up reaction of [**2**<sub>2</sub>]<sup>•-</sup> after electron transfer. In contrast to the behavior of [**2**<sub>2</sub>]<sup>2-</sup>, monomeric **1**<sup>-</sup> displays a (quasi)reversible oxidation at  $E_{1/2} = -535$  mV and an irreversible oxidation at  $E_p = +100$  mV.<sup>[16]</sup> This difference in reactivity will be discussed below.



Scheme 6. Oxidation of the aggregate [**2**<sub>2</sub>]<sup>2-</sup> to [**2**<sub>2</sub>]<sup>•-</sup> followed by proton transfer and dissociation to **H-2** and [**2a-H**]<sup>•-</sup>/[**2b-H**]<sup>•-</sup> radical anions.

Attempts to spectroscopically observe the radicals **2**<sup>•</sup> met with limited success due to the transient nature of these radical species. Independent of the preparative pathway (oxidation/deprotonation or deprotonation/oxidation), only EPR-silent reaction mixtures were obtained. However, the addition of approximately 1 equivalent of P<sub>1</sub>tBu to a pre-cooled solution (ca. 193 K) of [**H-2**]<sup>+</sup> and rapidly freezing the sample to 77 K delivered an EPR spectrum displaying a sharp resonance at  $g \approx 2.00$  and a

broad resonance at  $g \approx 1.96$  (see Figure S17 in the Supporting Information). We tentatively assigned the resonance at  $g \approx 2.00$  to the phenoxyl radical valence isomer [**2b**]<sup>•</sup> and/or the carbon-centered radicals [**2\***]<sup>•</sup> by comparison with the resonance of the phenoxyl radical **5**<sup>•</sup> and radicals [**3\***]<sup>•</sup> (see Table 2, Scheme 3, and Figure S18 in the Supporting Information). The high-field resonance is assigned to the ferrocenium part of the iminolate zwitterion [**2c**]<sup>•</sup> by comparison with the resonances of the ferrocenium iminolates [**1c**]<sup>•</sup> and [**3c**]<sup>•</sup> (Schemes 1, 3, 4, and Table 2).<sup>[16,26]</sup> Annealing this sample to room temperature for one minute and refreezing to 77 K resulted in an EPR-silent mixture. Clearly, the radicals **2**<sup>•</sup> are much more reactive than the radicals **1**<sup>•</sup> and they could not be observed by UV/Vis or IR spectroscopy.<sup>[16]</sup>

DFT geometry optimizations of the ferrocenium phenolate zwitterion [**2a**]<sup>•</sup>, the ferrocenyl phenoxyl radical [**2b**]<sup>•</sup>, and the ferrocenium iminolate zwitterion [**2c**]<sup>•</sup> showed that these valence isomers and tautomers are very close in energy (Figure 4). The quite high stability of the ferrocenium iminolate [**2c**]<sup>•</sup> can be accounted for by the increased acidity of the positively charged ferrocenium amides, similar to the stability of [**3c**]<sup>•</sup> (Scheme 3).<sup>[26,28,29]</sup> In contrast, zwitterion [**1a**]<sup>•</sup> is significantly stabilized relative to [**1b**]<sup>•</sup> and [**1c**]<sup>•</sup> due to its strong NH...O IHB.<sup>[16]</sup> The charge-transfer and d-d transitions of [**1a**]<sup>•</sup> and the elusive [**2a**]<sup>•</sup> derived by TD-DFT calculations can be compared in Table S2 in the Supporting Information.

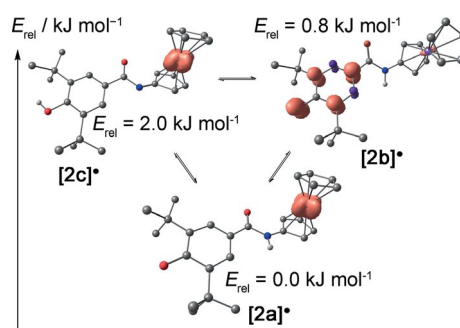


Figure 4. DFT-calculated geometries, energies, and spin densities (red, isosurface value 0.01 a.u.) of the valence isomers and tautomers of **2** (CH<sub>2</sub>Cl<sub>2</sub>; CH hydrogen atoms have been omitted).

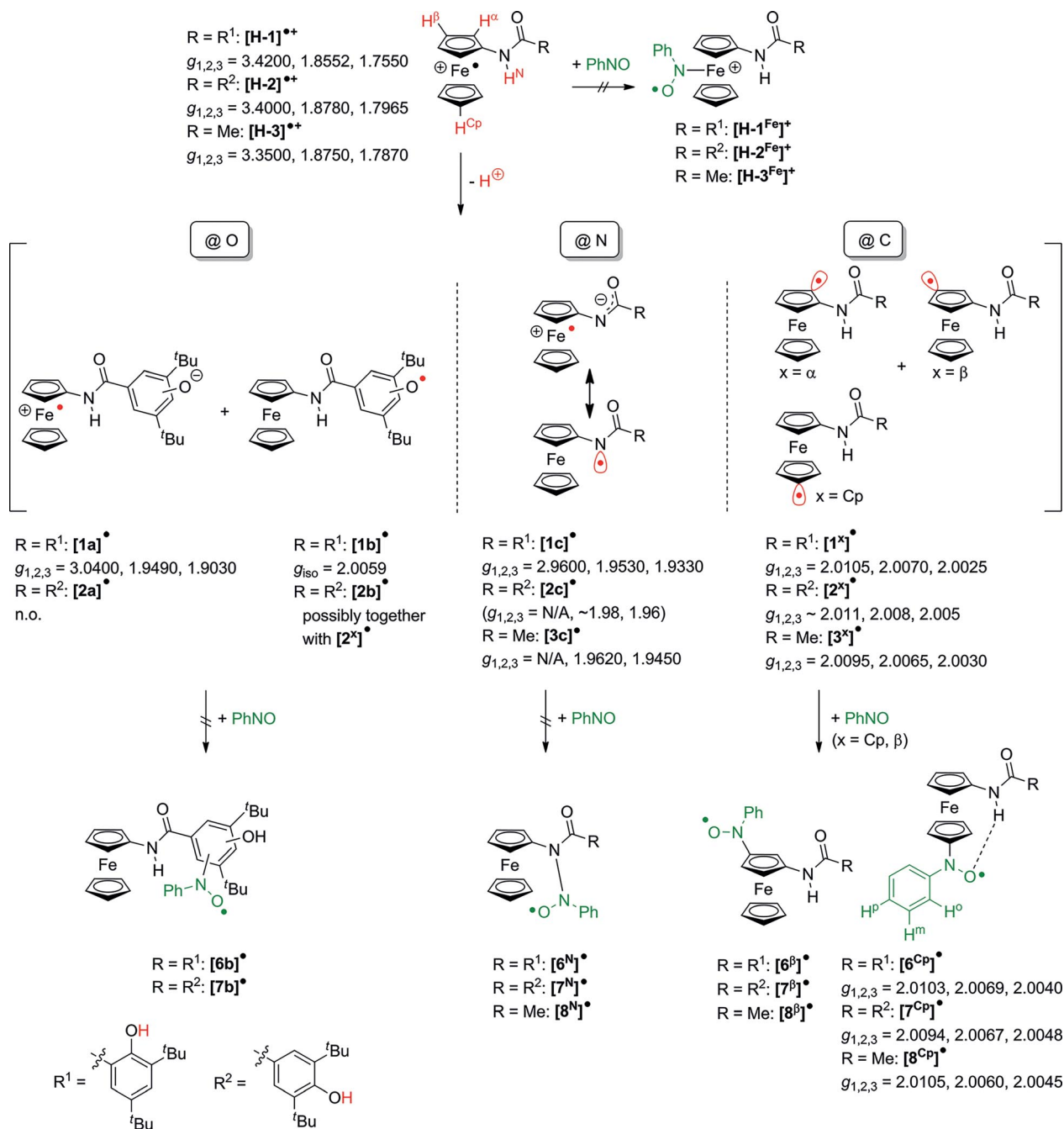
The high reactivity of **2**<sup>•</sup> in comparison with **1**<sup>•</sup> is not immediately obvious from the DFT calculations. The radicals [**2a**]<sup>•</sup>, [**2b**]<sup>•</sup>, and [**2c**]<sup>•</sup> should be quite persistent compared with typical phenoxyl and ferrocenium radicals such as **4**<sup>•</sup>, **5**<sup>•</sup>, FcH<sup>•</sup>, [**H-2**]<sup>•</sup>, and [**3c**]<sup>•</sup> (see Figures S18 and S13 in the Supporting Information and refs.<sup>[16,26,47–52]</sup>). The main difference between **1**<sup>•</sup> and **2**<sup>•</sup> is the type of NH...O hydrogen bond between the amide and phenolate in their precursor phenolates **1**<sup>-</sup> and **2**<sup>-</sup>, namely an intramolecular hydrogen bond in **1**<sup>-</sup> (Scheme 1) and an intermolecular hydrogen bond in **2**<sup>-</sup> ([**2**<sub>2</sub>]<sup>2-</sup>, Scheme 5, a). Given that **2**<sup>-</sup> forms (at least) dimeric aggregates [**2**<sub>2</sub>]<sup>2-</sup> in CH<sub>2</sub>Cl<sub>2</sub>/[*n*Bu<sub>4</sub>N][B(C<sub>6</sub>F<sub>5</sub>)<sub>4</sub>] solution (Scheme 5, a), the oxidation of this aggregate to [**2**<sub>2</sub>]<sup>•-</sup> should occur at the ferrocenyl moiety that forms the NH...O bond (Scheme 6) as this hydrogen bond increases the phenolate/phenoxyl potential but lowers the ferrocene/ferrocenium potential (see above).

In the radical aggregate  $[2_2]^-$ , a phenolate  $2^-$  is coordinated to the positively charged  $[\text{Fc-NH}]^{+\bullet}$  site of radical  $[2a]$ , which could easily result in a proton transfer from the acidic  $[\text{Fc-NH}]^{+\bullet}$  group to the phenolate. Dissociation furnishes **H-2** and the doubly deprotonated ferrocenium phenolate iminolate  $[2a-H]^-$  or the phenoxyl iminolate species  $[2b-H]^-$  (Scheme 6). The latter radical anions might be susceptible to decomposition. This mechanistic scenario fits perfectly with the electrochemical experiments (Figure 3): One-electron oxidation of the dimer  $[2_2]^{2-}$  ( $E_p = -500$  mV) leads to  $[2_2]^-$  followed by the formation of **H-2** ( $E_{1/2} = -110$  mV) and the follow-up products  $[2a-H]^-/[2b-H]^-$

( $E_p = 70$  mV). The  $[2_2]^{2-}/[2_2]^-$  redox process is followed by an intermolecular proton transfer leading to dissociation (EC mechanism). Oxidation of  $1^-$ , however, leads to stable  $[1a]$  with the hydrogen-bonded proton simply moving between the nitrogen and oxygen atoms.<sup>[16]</sup> To conclude, the fundamental difference in reactivity between  $2^-$  and  $1^-$  is based on the nature of the hydrogen bond.

### Spin-Trapping of Carbon-Centered Radicals

The ferrocenium iminolate  $[3c]$  equilibrates with a pool of carbon-centered radicals  $[3^x]$  ( $x = \alpha, \beta, \text{Cp}, \text{Me}$ ) and some of these



Scheme 7. Suggested radical reactivity of  $[\text{H-1}]^{+\bullet}$ ,  $[\text{H-2}]^{+\bullet}$ , and  $[\text{H-3}]^{+\bullet}$  in the presence of a base and PhNO. The EPR data (298 K, 77 K) of identified radical intermediates are given.

radicals can be intercepted by PhNO to give the nitroxides **[8<sup>Cp</sup>]** and **[8<sup>β</sup>]** (Scheme 3). Carbon-centered metallocenyl radicals might also be involved in the decarboxylation of cobaltocenium carboxylate.<sup>[53]</sup> Although PhNO has been reported to trap phenoxyl radicals,<sup>[54–57]</sup> the phenoxyl reference radicals **4<sup>•</sup>** and **5<sup>•</sup>** are inert towards PhNO under our conditions. Furthermore, simple ferrocenium ions such as FcH<sup>+</sup> or **[H-3]<sup>+</sup>** are also resistant towards PhNO.<sup>[26]</sup> Hence, the formation of nitroxide radicals selectively indicates the presence of ferrocenium iminolates, which equilibrate with C-centered radicals.

Indeed, **[H-1]<sup>+</sup>** and **[H-2]<sup>+</sup>** are unreactive towards PhNO and only the ferrocenium resonances are observed by EPR spectroscopy at 77 K (Table 2, Scheme 7). In the presence of base, the valence isomeric radicals **[1a]<sup>•</sup>**/**[2a]<sup>•</sup>** and **[1b]<sup>•</sup>**/**[2b]<sup>•</sup>** are formed (O deprotonation) along with the ferrocenium iminolates **[1c]<sup>•</sup>**/**[2c]<sup>•</sup>** (N deprotonation; Schemes 1, 4, a, and 7). The latter might equilibrate with C-centered radicals **[1<sup>x</sup>]<sup>•</sup>**/**[2<sup>x</sup>]<sup>•</sup>** (x = α, β, Cp; C deprotonation), which should be susceptible to the spin-trapping reaction giving nitroxide radicals **[6<sup>x</sup>]<sup>•</sup>**/**[7<sup>x</sup>]<sup>•</sup>** (Scheme 7). Indeed, EPR triplet resonances characteristic of nitroxide radicals are observed at 298 K in both cases (Figure 5) with a spectroscopic yield of less than 1 % (by double integration of the EPR resonance referenced against the DPPH radical).<sup>[26,39]</sup> The EPR parameters obtained for **[6<sup>x</sup>]<sup>•</sup>**/**[7<sup>x</sup>]<sup>•</sup>** closely resemble those of **[8<sup>Cp</sup>]** (Scheme 3, Table 1), which suggests a preferred substitution at the Cp ring (**[6<sup>Cp</sup>]<sup>•</sup>**/**[7<sup>Cp</sup>]<sup>•</sup>**) with possibly some substitution at the β position (**[6<sup>β</sup>]<sup>•</sup>**/**[7<sup>β</sup>]<sup>•</sup>**); Scheme 7). Similarly to the case of **[3<sup>x</sup>]<sup>•</sup>**/**[8<sup>x</sup>]<sup>•</sup>** and in agreement with DFT calculations, substitution at the nitrogen atom (**[6<sup>N</sup>]<sup>•</sup>**/**[7<sup>N</sup>]<sup>•</sup>**) is thermodynamically uphill whereas substitution reactions at the Cp ring and the α/β positions to give **[6<sup>Cp,α,β</sup>]<sup>•</sup>** and **[7<sup>Cp,α,β</sup>]<sup>•</sup>** are thermodynamically feasible (Figure 6). The driving forces are similar for the **[6<sup>Cp,α,β</sup>]<sup>•</sup>** and **[7<sup>Cp,α,β</sup>]<sup>•</sup>** nitroxides derived from the radicals **[1<sup>x</sup>]<sup>•</sup>**/**[2<sup>x</sup>]<sup>•</sup>** (Scheme 7). According to DFT calculations, the conceivable nitroxide radicals **[6b]<sup>•</sup>**/**[7b]<sup>•</sup>** derived from the phenoxyl radicals **[1b]<sup>•</sup>**/**[2b]<sup>•</sup>** are thermodynamically unfavorable with respect to the starting radical and PhNO (see Figures S19 and S20 in the Supporting Information), in agreement with the experimental observations that the phenoxyl radicals **4<sup>•</sup>** and **5<sup>•</sup>** are inert towards nitroxide radical formation with PhNO (see above).

DFT calculations were also performed on the radicals **[1<sup>x</sup>]<sup>•</sup>**/**[2<sup>x</sup>]<sup>•</sup>** (x = α, β, Cp; see Figures S21 and S22 in the Supporting Information). As expected, all these radicals are high-energy species, independent of the presence or absence of NH...O or OH...O IHBs. The spin densities in radicals **[1<sup>α</sup>]<sup>•</sup>** and **[2<sup>α</sup>]<sup>•</sup>** are essentially localized at the iron center (Mulliken spin density at iron: 1.25/1.25), which suggests a dominant contribution of a ferrocenium carbanion resonance structure, similar to **[3<sup>α</sup>]<sup>•</sup>**.<sup>[26]</sup> Hence, a reaction of **[1<sup>α</sup>]<sup>•</sup>**/**[2<sup>α</sup>]<sup>•</sup>** with PhNO is not expected. In contrast, **[1<sup>Cp</sup>]<sup>•</sup>**/**[2<sup>Cp</sup>]<sup>•</sup>** and **[1<sup>β</sup>]<sup>•</sup>**/**[2<sup>β</sup>]<sup>•</sup>** feature large spin densities at the respective carbon atoms with Mulliken spin densities above 0.65 and hence should be susceptible to attack by PhNO. This is essentially independent of the type of IHB (NH...O, OH...O) in the radicals **[1<sup>x</sup>]<sup>•</sup>** (see Figures S21 and S22 in the Supporting Information).

The presence of **[1<sup>x</sup>]<sup>•</sup>** and **[2<sup>x</sup>]<sup>•</sup>** radicals has been probed by rapid-freeze EPR techniques. Indeed, adding P<sub>1</sub>tBu to a pre-

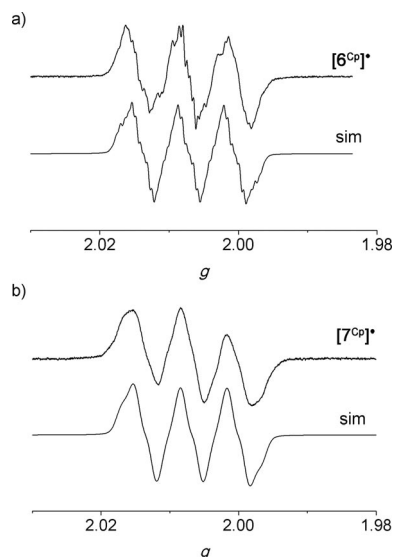


Figure 5. X-band EPR spectra (top) and simulated spectra (bottom) of a) **[6<sup>Cp</sup>]<sup>•</sup>** (25 mM) in CH<sub>2</sub>Cl<sub>2</sub> and b) **[7<sup>Cp</sup>]<sup>•</sup>** (3 mM) in CH<sub>2</sub>Cl<sub>2</sub>. All the spectra were recorded by using the following parameters: *T* = 298 K, field: 3346.20 G, sweep: 94.79 G, sweep time: 90 s, modulation: 250 mG, MW attenuation: 5 dB (**[6<sup>Cp</sup>]<sup>•</sup>**) and modulation: 5000 mG, MW attenuation: 10 dB (**[7<sup>Cp</sup>]<sup>•</sup>**).

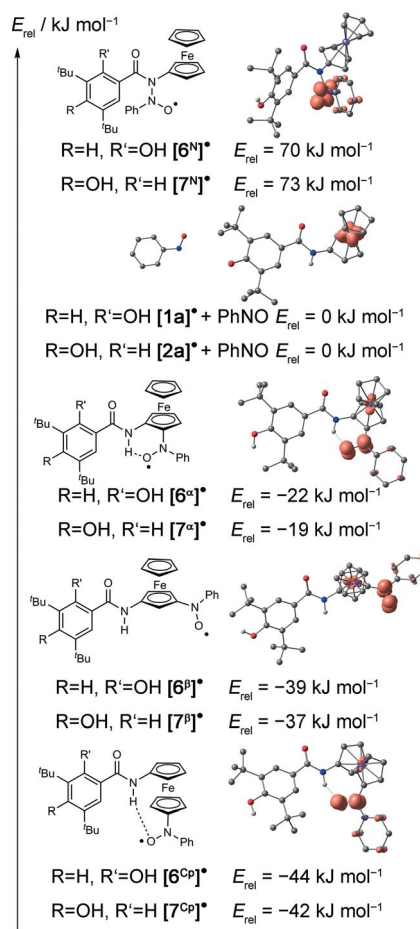


Figure 6. DFT-optimized geometries with spin densities for **[7<sup>x</sup>]<sup>•</sup>** (x = α, β, Cp, N) (0.01 a.u. isosurface value) and energies in CH<sub>2</sub>Cl<sub>2</sub> continuum solvent for **[6<sup>x</sup>]<sup>•</sup>** and **[7<sup>x</sup>]<sup>•</sup>** (x = N, α, β, Cp) as well as their Lewis structures.

cooled solution containing  $[\mathbf{H-1}]^+$  and PhNO (ca. 193 K) and rapid freezing to 77 K allowed the detection of a broad, anisotropic large ferrocenium resonance at around  $g = 1.96$  (98.7 %) as well as a sharp resonance signal at around  $g = 2.00$  without discernible hfc constants (1.3 %; Table 2; Figure 7, a). The former closely resembles the resonance of the ferrocenium iminolate  $[\mathbf{3c}]$ ; whereas the latter is similar to that of the carbon-centered radicals  $[\mathbf{3}^{\text{Cp},\beta}]$  (Table 2, Schemes 3 and 7).<sup>[26]</sup> Hence, we assigned the former to the ferrocenium iminolate zwitterion  $[\mathbf{1c}]$  and the latter to traces of the radicals  $[\mathbf{1}^{\text{Cp},\beta}]$ . Clearly,  $[\mathbf{H-1}]^+$  is deprotonated mainly at the amide nitrogen atom to give the ferrocenium iminolate  $[\mathbf{1c}]$  and to some extent at the Cp rings to give  $[\mathbf{1}^{\text{Cp},\beta}]$  as the phenolic OH is engaged in an OH...O IHB (Scheme 1). On this time scale, the kinetic product  $[\mathbf{1c}]$  has not yet been quantitatively isomerized to radicals  $[\mathbf{1a}]$  and  $[\mathbf{1b}]$ .

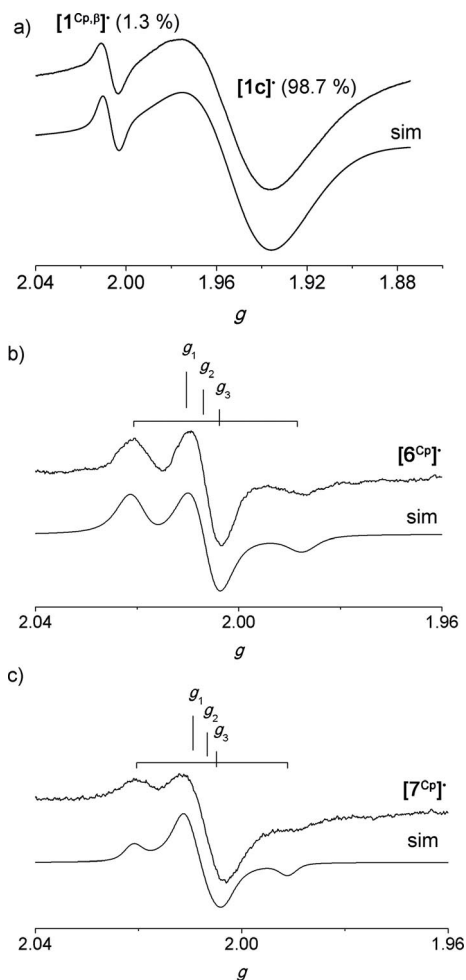
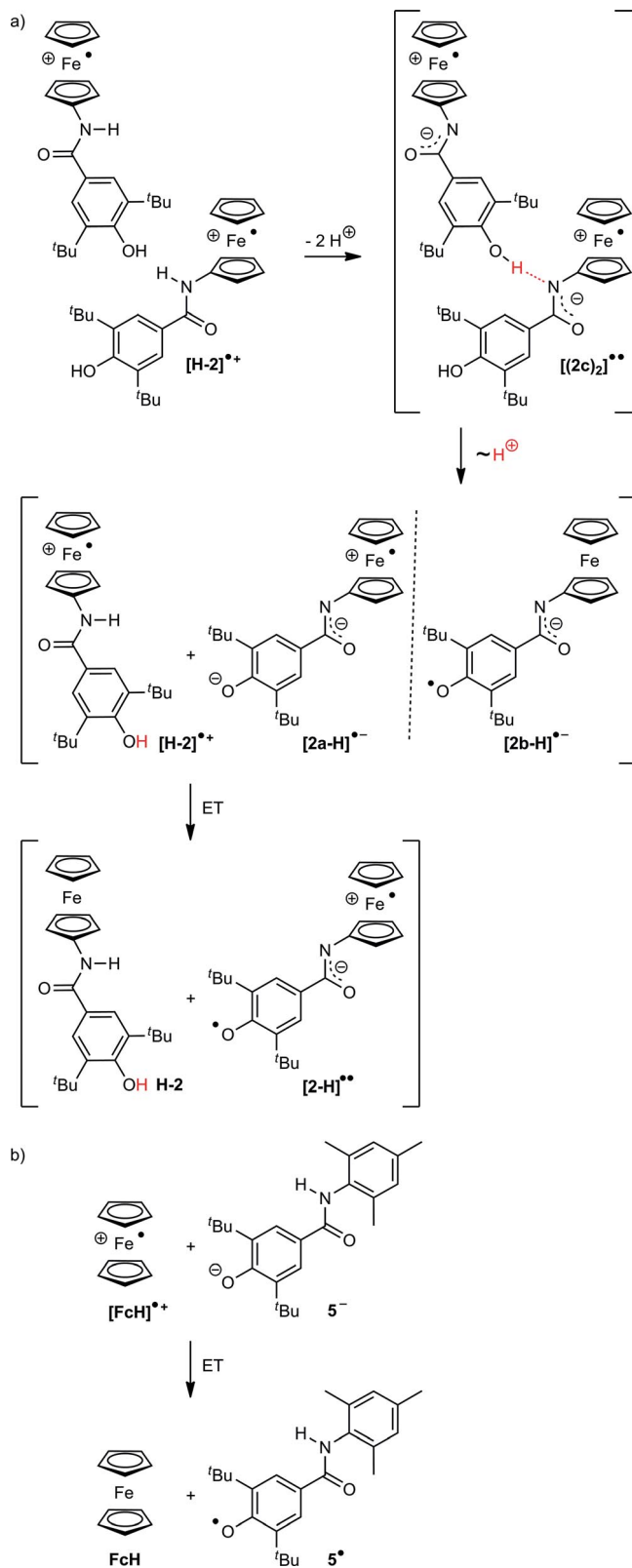


Figure 7. X-band EPR spectra (top) and simulated spectra (bottom) of a) a rapidly frozen mixture of  $[\mathbf{1}^{\text{Cp},\beta}]/[\mathbf{1c}]$  (25 mM  $\mathbf{H-1}$ ) in  $\text{CH}_2\text{Cl}_2$ , b)  $[\mathbf{6}^{\text{Cp}}]$  (25 mM  $\mathbf{H-1}$ ) in  $\text{CH}_2\text{Cl}_2$  after annealing at room temperature, and c)  $[\mathbf{7}^{\text{Cp}}]$  (3.0 mM  $\mathbf{H-2}$ ) in  $\text{CH}_2\text{Cl}_2/[n\text{Bu}_4\text{N}][\text{B}(\text{C}_6\text{F}_5)_4]$ . All the spectra were recorded by using the following parameters: temperature = 77 K, field = 3346.20 G, sweep = 499.77 G, sweep time = 90 s, modulation = 5000 mG, MW attenuation = 20 dB ( $[\mathbf{1}^{\text{Cp},\beta}]/[\mathbf{1c}]$  and  $[\mathbf{6}^{\text{Cp}}]$ ) and 10 dB ( $[\mathbf{7}^{\text{Cp}}]$ ).

No nitroxide radicals were discernible in this sample. Clearly, the following trapping reaction of  $[\mathbf{1}^{\text{Cp},\beta}]$  with PhNO is slow enough to allow detection of radicals  $[\mathbf{1}^{\text{Cp},\beta}]$ . After annealing the sample to room temperature for five minutes and refreezing



Scheme 8. a) Possible deprotonation of the ferrocenium ion  $[\mathbf{H-2}]^+$  to give the dimeric aggregate  $[(\mathbf{2c})_2]^{2-}$ , followed by proton transfer and dissociation into  $[\mathbf{H-2}]^+$  and  $[\mathbf{2a-H}]^-/[\mathbf{2b-H}]^-$  with subsequent electron transfer to give  $\mathbf{H-2}$  and diradical  $[\mathbf{2-H}]^{\bullet}$ . b) Oxidation of phenolate  $\mathbf{5}^-$  with the ferrocenium ion  $[\mathbf{FcH}]^+$ .

to 77 K, the  $[1c]^\cdot$  and  $[1^{CP,\beta}]^\cdot$  resonances vanished in favor of the nitroxide EPR resonance of  $[6^{CP,\beta}]^\cdot$  with a large nitrogen hfc for the  $g_3$  resonance, similar to nitroxide radicals  $[8^{CP,\beta}]^\cdot$  (Table 2, Figure 7, b).

The rapid-freeze EPR spectrum (77 K) of a mixture of  $[H-2]^{+\cdot}$ , PhNO, and  $P_1tBu$ , prepared as described for  $[H-1]^{+\cdot}$  yielded only the resonance of the nitroxide radicals  $[7^{CP,\beta}]^\cdot$  without indication of ferrocenium phenolate  $[2a]^\cdot$ , phenoxy radical  $[2b]^\cdot$ , ferrocenium iminolate  $[2c]^\cdot$ , or C-centered radicals  $[2^{CP,\beta}]^\cdot$  (Figure 7, c). Hence, under these conditions, the follow-up reactions are too fast and only some  $[2^{CP,\beta}]^\cdot$  radicals have been intercepted by PhNO to yield  $[7^{CP,\beta}]^\cdot$  (Scheme 7). Again, a conceivable follow-up reaction of  $[2c]^\cdot$  and its conceivable hydrogen-bonded dimer  $[(2c)_2]^\cdot$  (Scheme 8) might be intermolecular proton transfer from the phenol to the iminolate to give ferrocenium cation  $[H-2]^{+\cdot}$  and the doubly deprotonated ferrocenium phenolate iminolate  $[2a-H]^\cdot$  or phenoxy iminolate species  $[2b-H]^\cdot$  (similar to the reactivity of  $[2_2]^\cdot$ , Scheme 6). As the ferrocenium ion  $[FCH]^{+\cdot}$  oxidizes phenolate  $5^-$  to the phenoxy radical  $5^\cdot$  (Scheme 8, b), a similar reaction might occur between  $[H-2]^{+\cdot}$  and the proposed doubly deprotonated ferrocenium phenolate iminolate  $[2a-H]^\cdot$  to give diradical  $[2-H]^\cdot$  (Scheme 8, a). Such a diradical might be prone to decomposition yielding only EPR-silent products.

## Conclusions

Amide-bridged ferrocenyl phenols **H-1** and **H-2** can be oxidized to the respective ferrocenium phenol radical cations  $[H-1]^{+\cdot}$  and  $[H-2]^{+\cdot}$ , respectively. These are deprotonated at the phenol oxygen atom, the amide nitrogen atom, or cyclopentadienyl carbon atoms to give the corresponding neutral radicals  $[1a]^\cdot/[2a]^\cdot$ ,  $[1b]^\cdot/[2b]^\cdot$  (@O),  $[1c]^\cdot/[2c]^\cdot$  (@N), and  $[1x]^\cdot/[2x]^\cdot$  (@C; Scheme 7). The ferrocenium iminolate  $[1c]^\cdot$  and the carbon-centered radicals  $[1^{CP,\beta}]^\cdot$  are the kinetic products of the  $[H-1]^{+\cdot}$  deprotonation. The latter species are intercepted by PhNO as nitroxide radicals  $[6^{CP,\beta}]^\cdot$ . The  $NH\cdots O$  IHB in  $[1a]^\cdot$  strongly stabilizes the ferrocenium phenolate zwitterion, yet traces of the valence isomeric phenoxy radical  $[1b]^\cdot$  are also observed at 298 K. The IVCT between  $[1a]^\cdot$  and  $[1b]^\cdot$  is coupled to the  $NH\cdots O$  vibration. For  $[H-2]^{+\cdot}$  lacking IHBs, all the radicals derived by deprotonation are transient. Only some of them can be observed by rapid-freeze EPR techniques ( $[2b]^\cdot$ ;  $[2c]^\cdot$ ) or indirectly by spin-trapping techniques ( $[2^{CP,\beta}]^\cdot$  as  $[7^{CP,\beta}]^\cdot$ ). Suggested follow-up reactions of these transient radicals  $2^\cdot$  are intermolecular proton (and electron) transfer reactions in hydrogen-bonded assemblies leading finally to EPR-silent products. This contrasts with the reversible intramolecular PCET reaction (IVCT) between  $[1a]^\cdot$  and  $[1b]^\cdot$ . The absence of the stabilizing IHB and the resulting high reactivity precludes the observation of IVCT between the transient valence isomers  $[2a]^\cdot$  and  $[2b]^\cdot$ . In any case, ferrocenyl phenols generate a pool of radicals under oxidative and basic conditions. This observation might also be relevant for biologically active ferrocenyl phenols such as ferrocifen (**H-C**).

## Experimental Section

**General:** All reactions were performed under argon unless noted otherwise. Dichloromethane was dried with  $CaH_2$  and distilled prior

to use. Absolute DMF was used as received from Acros. 1-[Bis(dimethylamino)methylene]-1*H*-1,2,3-triazolo[4,5-*b*]pyridinium 3-oxide hexafluorophosphate (HATU) was commercially available from Novabiochem.  $P_1tBu$ , sodium hydroxide, 2,6-di-*tert*-butyl-4-carboxyphenol, *N,N*-diisopropylethylamine (DIPEA), 2,2-diphenyl-1-picrylhydrazyl (DPPH), nitrosobenzene (PhNO), ferrocenium hexafluorophosphate, decamethylcobaltocene, and 2,4,6-trimethylaniline were commercially available from Sigma-Aldrich. DIPEA was dried with NaOH overnight under argon and applied to the coupling reactions through a syringe. Aminoferrocene,<sup>[27,34]</sup> 2,4-di-*tert*-butyl-6-(ferrocenylcarbamoyl)phenol (**H-1**),<sup>[16]</sup> 2,4-di-*tert*-butyl-6-(methylcarbamoyl)phenol (**H-4**),<sup>[25]</sup> *N*-acetylaminoferrocene (**H-3**),<sup>[27]</sup> and  $[nBu_4N][B(C_6F_5)_4]^{[44]}$  were prepared according to literature procedures.

Filtrations from precipitated silver after oxidation were performed with syringe filters (Rotilabo-Spritzenfilter,  $\varnothing = 15$  mm, pore size: 0.20  $\mu m$ ; Carl Roth GmbH + Co. KG, Germany). NMR spectra were recorded with a Bruker Avance DRX 400 spectrometer at 400.13 ( $^1H$ ) and 100.03 MHz ( $^{13}C\{^1H\}$ ) at 25 °C. All resonances are reported in ppm versus the solvent signal as internal standard:  $CD_2Cl_2$  ( $^1H$ :  $\delta = 5.32$  ppm;  $^{13}C$ :  $\delta = 54.0$  ppm),  $CDCl_3$  ( $^1H$ :  $\delta = 7.26$  ppm;  $^{13}C$ :  $\delta = 77.2$  ppm), and  $[D_8]THF$  ( $^1H$ :  $\delta = 3.58$  ppm;  $^{13}C$ :  $\delta = 67.6$  ppm). IR spectra were recorded with a Varian Excalibur Series 3100 FT-IR spectrometer using KBr cells in  $CH_2Cl_2$  and as KBr disks. Electrochemical experiments were carried out with a BioLogic SP-50 voltammetric analyzer using a platinum working electrode, a platinum wire as counter electrode, and a 0.01 M  $Ag/AgNO_3$  electrode as reference electrode. The measurements were carried out at a scan rate of 100  $mV s^{-1}$  for cyclic and square-wave voltammetry experiments unless noted otherwise using 0.1 M  $[nBu_4N][B(C_6F_5)_4]$  as supporting electrolyte and 0.001 M of the sample in  $CH_2Cl_2$ . Potentials are given relative to the ferrocene/ferrocenium couple. Referencing was achieved by addition of decamethylcobaltocene ( $E_{1/2} = -2.04$  V vs.  $FcH/FcH^+$ ,  $CH_2Cl_2$ ,  $[nBu_4N][B(C_6F_5)_4]$ ) to the sample.<sup>[36]</sup> UV/Vis/NIR spectra were recorded with a Varian Cary 5000 spectrophotometer using 1.0 cm cells unless mentioned otherwise (Hellma, Suprasil). FD mass spectra were recorded with a Thermo Fisher DFS mass spectrometer with a LIFDI upgrade. CW EPR spectra (X-band; ca. 9.4 GHz) were recorded with a Miniscope MS 300 spectrometer at 298 and 77 K with cooling in liquid nitrogen in a finger Dewar (Magnettech GmbH, Berlin, Germany). Settings are given as indicated in the spectra. The  $g$  factors are referenced to external  $Mn^{2+}$  in ZnS ( $g = 2.118, 2.066, 2.027, 1.986, 1.946, 1.906$ ). The EPR spectra were simulated by using EasySpin (v 5.0.0)<sup>[58]</sup> for MatLab (R2015a). Melting points were determined by using a Gallenkamp capillary melting point apparatus (MFB 595 010M). Elemental analyses were performed by the microanalytical laboratory of the chemical institutes of the University of Mainz.

**Crystal Structure Determination:** Intensity data were collected with a Bruker AXS Smart1000 CCD diffractometer equipped with an APEX II detector and an Oxford cooling system using  $Mo-K_{\alpha}$  radiation ( $\lambda = 0.71073$  Å) at 173(2) K and were corrected for absorption and other effects. The diffraction frames were integrated by using the SAINT software package, and most were corrected for absorption with MULABS.<sup>[59,60]</sup> The structures were solved by direct methods and refined by the full-matrix method based on  $F^2$  using the SHELXTL software package.<sup>[61,62]</sup> All non-hydrogen atoms were refined anisotropically, and the positions of all hydrogen atoms were generated with appropriate geometric constraints and allowed to ride on their respective parent atoms with fixed isotropic thermal parameters.

CCDC 1426154 (for **H-1**) contains the supplementary crystallographic data for this paper. These data can be obtained free of charge from The Cambridge Crystallographic Data Centre.

**Density Functional Calculations:** DFT calculations were carried out with the ORCA 3.0.2/DFT series<sup>[63]</sup> of programs. For geometry optimizations and energy calculations, the B3LYP formulation of density functional theory was used employing the SV(P)<sup>[64,65]</sup> basis set, the RIJCOSX approximation, the approximate second order SCF (SOSCF),<sup>[66,67]</sup> the zero-order regular approximation (ZORA),<sup>[68–70]</sup> and the KDIIIS algorithm at GRIDX4. No symmetry constraints were imposed on the molecules. Solvent modeling was carried out by employing the conductor-like screening model (COSMO, CH<sub>2</sub>Cl<sub>2</sub>).<sup>[71]</sup> The approximate free energies at 298 K were obtained by thermochemical analysis of the frequency calculations using the thermal correction to Gibbs free energy as reported by ORCA 3.0.2. TD-DFT calculations were performed by using the same basis set and functional as for the geometry optimizations, calculating 50 states with MaxDim = 250. The 4-methyl group of **H-5** and all its ET and PT products were omitted from the DFT calculations for convergence reasons.

**2,6-Di-tert-butyl-4-(ferrocenylcarbamoyl)phenol (H-2):** Aminoferrocene (250 mg, 1.24 mmol, 1.0 equiv.) and 2,6-di-tert-butyl-4-carboxyphenol (311 mg, 1.24 mmol, 1.0 equiv.) were dissolved in absolute CH<sub>2</sub>Cl<sub>2</sub> (10 mL). DIPEA (241 mg, 320 μL, 1.87 mmol, 1.5 equiv.) was added to the mixture followed by HATU (472 mg, 1.243 mmol, 1.0 equiv.). The solution was stirred at room temperature for 2 h. Water (10 mL) was added and the product was extracted with CH<sub>2</sub>Cl<sub>2</sub> (3 × 30 mL). The organic phase was washed with water (10 mL) and brine (10 mL) and dried with MgSO<sub>4</sub>. After filtration the solvent was removed under reduced pressure. The raw product was purified by column chromatography [SiO<sub>2</sub>, petroleum ether (40–60 °C)/CH<sub>2</sub>Cl<sub>2</sub>, 1:0 → 1:4] to give a yellow solid, yield 79 % (423 mg, 0.98 mmol). *R*<sub>f</sub> (CH<sub>2</sub>Cl<sub>2</sub>) = 0.17, m.p. > 350 °C (decomp.). *E*<sub>1/2</sub> = –105 mV. <sup>1</sup>H NMR (CD<sub>2</sub>Cl<sub>2</sub>): δ = 7.60 (s, 2 H, 7-H), 7.09 (s, 1 H, NH), 5.63 (s, 1 H, OH), 4.71 (s, 2 H, 2,5-H), 4.18 (s, 5 H, Cp), 4.05 (s, 2 H, 3,4-H), 1.48 (s, 18 H, 10a-H) ppm. <sup>1</sup>H NMR ([D<sub>8</sub>]THF): δ = 8.50 (s, 1 H, OH), 7.73 (s, 2 H, 7-H), 6.59 (s, 1 H, NH), 4.74 (pt, 2 H, 2,5-H), 4.09 (s, 5 H, Cp), 3.92 (pseudo-t, 2 H, 3,4-H), 1.47 (s, 18 H, 10a-H) ppm. <sup>13</sup>C NMR (CD<sub>2</sub>Cl<sub>2</sub>): δ = 157.4 (C-9), 136.7 (C-8), 124.6 (C-7), 69.8 (Cp), 65.1 (C-3,4), 62.1 (C-2,5), 34.9 (C-10), 30.5 (C-10a) ppm. <sup>13</sup>C NMR ([D<sub>8</sub>]THF): δ = 166.3 (C=O), 157.8 (C-9), 137.6 (C-8), 127.8 (C-6), 125.4 (C-7), 98.4 (C-1), 68.8 (Cp), 64.7 (C-3,4), 61.7 (C-2,5), 35.5 (C-10), 30.7 (C-10a) ppm. UV/Vis/NIR (CH<sub>2</sub>Cl<sub>2</sub>): λ (ε) = 230 (13825), 257 (16785), 325 (1815), 440 nm (325 m<sup>-1</sup> cm<sup>-1</sup>). IR (KBr): ν̄ = 3625 (m, OH), 3285 (m, NH), 1635 (m, CO) cm<sup>-1</sup>. IR (CH<sub>2</sub>Cl<sub>2</sub>): ν̄ = 3625 (m, OH), 3440 (m, NH), 1665 (m, CO) cm<sup>-1</sup>. MS (FD): *m/z* (%) = 433.2 (100), 434.2 (28.7) [M]<sup>+</sup>, 866.2 (11.8) [2M]<sup>+</sup>. C<sub>25</sub>H<sub>31</sub>FeNO<sub>2</sub> (433.17): calcd. C 69.29, H 7.21, N 3.23; found C 69.64, H 7.48, N 3.41.

**2,6-Di-tert-butyl-4-(2,4,6-trimethylphenylcarbamoyl)phenol (H-5):** 2,4,6-Trimethylaniline (168 mg, 174 μL, 1.24 mmol, 1.0 equiv.) and 2,6-di-tert-butyl-4-carboxyphenol (311 mg, 1.24 mmol, 1.0 equiv.) were dissolved in CH<sub>2</sub>Cl<sub>2</sub> (15 mL). DIPEA (241 mg, 320 μL, 1.87 mmol, 1.5 equiv.) was added to the mixture followed by HATU (472 mg, 1.243 mmol, 1.0 equiv.). The solution was stirred at room temperature for 2 h. Water (15 mL) was added and the solution was extracted with CH<sub>2</sub>Cl<sub>2</sub> (2 × 30 mL). The organic phase was washed with a saturated aqueous sodium hydrogen carbonate solution (15 mL) and brine (15 mL) and dried with MgSO<sub>4</sub>. After filtration, the solvent was removed under reduced pressure. The raw product was purified by column chromatography [SiO<sub>2</sub>, CH<sub>2</sub>Cl<sub>2</sub>/MeOH, 1:0 → 95:5] to give a colorless solid, yield 72 % (328 mg, 0.89 mmol). *R*<sub>f</sub> (CH<sub>2</sub>Cl<sub>2</sub>/MeOH, 98:2) = 0.47, m.p. 301–303 °C (decomp.). <sup>1</sup>H NMR

(CDCl<sub>3</sub>): δ = 7.75 (s, 2 H, 7-H), 7.18 (s, 1 H, NH), 6.93 (s, 2 H, 3-H), 5.60 (s, 1 H, OH), 2.29 (s, 3 H, 5b-H), 2.25 (s, 6 H, 5a-H), 1.49 (s, 18 H, 10a-H) ppm. <sup>13</sup>C NMR (CDCl<sub>3</sub>): δ = 166.6 (C=O), 157.2 (C-9), 137.0 (C-4), 136.2 (C-8), 135.4 (C-2), 131.7 (C-1), 129.1 (C-3), 126.0 (C-6), 124.6 (C-7), 34.6 (C-10), 30.3 (C-10a), 21.1 (C-5b), 18.7 (C-5a) ppm. UV/Vis/NIR (CH<sub>2</sub>Cl<sub>2</sub>): λ (ε) = 275 nm (15800 m<sup>-1</sup> cm<sup>-1</sup>). IR (KBr): ν̄ = 3625 (m, OH), 3190 (m, NH), 1635 (m, CO) cm<sup>-1</sup>. IR (CH<sub>2</sub>Cl<sub>2</sub>): ν̄ = 3625 (m, OH), 3425 (m, NH), 1665 (m, CO) cm<sup>-1</sup>. MS (FD): *m/z* (%) = 367.2 (100) [M]<sup>+</sup>. C<sub>24</sub>H<sub>33</sub>NO<sub>2</sub> (367.25): calcd. C 78.43, H 9.05, N 3.81; found C 78.16, H 9.31, N 3.73.

**Electron Transfer Between Ferrocenium Hexafluorophosphate ([Fch][PF<sub>6</sub>]) and Phenolate 5<sup>-</sup>:** A stoichiometric amount of a solution of [Fch][PF<sub>6</sub>] was added to a solution of 5<sup>-</sup> in CH<sub>2</sub>Cl<sub>2</sub>/[*n*Bu<sub>4</sub>N][B(C<sub>6</sub>F<sub>5</sub>)<sub>4</sub>]. An immediate color change from blue to orange (Fch) was observed. The EPR spectra of a sample of this solution recorded at 298 and 77 K show resonances arising from 5<sup>-</sup> (see Figure S18 in the Supporting Information).

## Acknowledgments

The authors are grateful to Regine Jung-Pothmann for the X-ray data collection, Dipl.-Chem. Torben Kienz for helpful discussions, as well as Dipl.-Chem. Mathias Enders and Dipl.-Chem. Maximilian Lauck for preparative assistance. Parts of this research were conducted using the supercomputer Mogon and the advisory services offered by Johannes Gutenberg-University Mainz (www.hpc.uni-mainz.de), which is a member of the AHRP and the Gauss Alliance e.V.

**Keywords:** Hydrogen bonds · Charge transfer · Radicals · EPR spectroscopy · Sandwich complexes · Valence isomers

- [1] R. A. Marcus, N. Sutin, *Biochim. Biophys. Acta Rev. Bioenerg.* **1985**, *811*, 265–322.
- [2] G. L. Closs, J. R. Miller, *Science* **1988**, *240*, 440–447.
- [3] J. R. Winkler, H. B. Gray, *Annu. Rev. Biochem.* **1996**, *65*, 537–561.
- [4] P. F. Barbara, T. J. Meyer, M. A. Ratner, *J. Phys. Chem.* **1996**, *100*, 13148–13168.
- [5] T. Kienz, C. Förster, K. Heinze, *Organometallics* **2014**, *33*, 4803–4812.
- [6] M. A. Fox, *Chem. Rev.* **1992**, *92*, 365–368.
- [7] C. Creutz, H. Taube, *J. Am. Chem. Soc.* **1969**, *91*, 3988–3989.
- [8] T. F. Markle, J. M. Mayer, *Angew. Chem. Int. Ed.* **2008**, *47*, 738–740; *Angew. Chem.* **2008**, *120*, 750–752.
- [9] J. J. Warren, T. A. Tronic, J. M. Mayer, *Chem. Rev.* **2010**, *110*, 6961–7001.
- [10] a) J.-M. Savéant, *Energy Environ. Sci.* **2012**, *5*, 7718–7731; b) C. Costentin, M. Robert, J.-M. Savéant, *Phys. Chem. Chem. Phys.* **2010**, *12*, 11179–11190.
- [11] a) S. Hammes-Schiffer, *Chem. Rev.* **2010**, *110*, 6937–6938; b) S. Hammes-Schiffer, A. Stuchebrukhov, *Chem. Rev.* **2010**, *110*, 6939–6960; c) S. Hammes-Schiffer, *J. Am. Chem. Soc.* **2015**, *137*, 8860–8871.
- [12] I. J. Rhile, T. F. Markle, H. Nagao, A. G. DiPasquale, O. P. Lam, M. A. Lockwood, K. Rotter, J. M. Mayer, *J. Am. Chem. Soc.* **2006**, *128*, 6075–6088.
- [13] a) O. S. Wenger, *Chem. Eur. J.* **2011**, *17*, 11692–11702; b) W. Herzog, C. Bronner, S. Löffler, B. He, D. Kratzert, D. Stalke, A. Hauser, O. S. Wenger, *ChemPhysChem* **2013**, *14*, 1168–1176.
- [14] D. R. Weinberg, C. J. Gagliardi, J. F. Hull, C. F. Murphy, C. A. Kent, B. C. Westlake, A. Paul, D. H. Ess, D. G. McCafferty, T. J. Meyer, *Chem. Rev.* **2012**, *112*, 4016–4093.
- [15] C. Costentin, M. Robert, J.-M. Savéant, *J. Am. Chem. Soc.* **2006**, *128*, 4552–4553.
- [16] A. Neidlinger, V. Ksenofontov, K. Heinze, *Organometallics* **2013**, *32*, 5955–5965.

- [17] M. H. V. Huynh, T. J. Meyer, *Chem. Rev.* **2007**, *107*, 5004–5064.
- [18] J. L. Dempsey, J. R. Winkler, H. B. Gray, *Chem. Rev.* **2010**, *110*, 7024–7039.
- [19] F. Lachaud, A. Quaranta, Y. Pellegrin, P. Dorlet, M.-F. Charlot, S. Un, W. Leibl, A. Aukauloo, *Angew. Chem. Int. Ed.* **2005**, *44*, 1536–1540; *Angew. Chem.* **2005**, *117*, 1560–1564.
- [20] J. Bonin, M. Robert, *Photochem. Photobiol.* **2011**, *87*, 1190–1203.
- [21] L. Hammarström, S. Styring, *Energy Environ. Sci.* **2011**, *4*, 2379–2388.
- [22] C. J. Gagliardi, A. K. Vannucci, J. J. Concepcion, Z. Chen, T. J. Meyer, *Energy Environ. Sci.* **2012**, *5*, 7704–7717.
- [23] A. Migliore, N. F. Polizzi, M. J. Therien, D. N. Beratan, *Chem. Rev.* **2014**, *114*, 3381–3465.
- [24] M. Sugiura, S. Ogami, M. Kusumi, S. Un, F. Rappaport, A. Boussac, *J. Biol. Chem.* **2012**, *287*, 13336–13347.
- [25] R. Wanke, L. Benisvy, M. L. Kuznetsov, M. F. C. Guedes Da Silva, A. J. L. Pombeiro, *Chem. Eur. J.* **2011**, *17*, 11882–11892.
- [26] A. Neidlinger, T. Kienz, K. Heinze, *Organometallics* **2015**, *34*, 5310–5320.
- [27] K. Heinze, M. Schlenker, *Eur. J. Inorg. Chem.* **2004**, 2974–2988.
- [28] a) K. Heinze, D. Siebler, *Z. Anorg. Allg. Chem.* **2007**, *633*, 2223–2233; b) D. Siebler, M. Linseis, T. Gasi, L. M. Carrella, R. F. Winter, C. Förster, K. Heinze, *Chem. Eur. J.* **2011**, *17*, 4540–4551.
- [29] D. Siebler, C. Förster, K. Heinze, *Dalton Trans.* **2011**, *40*, 3558–3575.
- [30] H. Huesmann, C. Förster, D. Siebler, T. Gasi, K. Heinze, *Organometallics* **2012**, *31*, 413–427.
- [31] M. B. Robin, P. Day, *Adv. Inorg. Chem. Radiochem.* **1968**, *10*, 247–422.
- [32] a) S. Fukuzumi, K. Okamoto, Y. Yoshida, H. Imahori, Y. Araki, O. Ito, *J. Am. Chem. Soc.* **2003**, *125*, 1007–1013; b) S. Fukuzumi, Y. Yoshida, K. Okamoto, H. Imahori, Y. Araki, O. Ito, *J. Am. Chem. Soc.* **2002**, *124*, 6794–6795.
- [33] a) G. Jaouen, S. Top, A. Vessieres, G. Leclercq, M. McGlinchey, *Curr. Med. Chem.* **2004**, *11*, 2505–2517; b) E. Hillard, A. Vessières, L. Thouin, G. Jaouen, C. Amatore, *Angew. Chem. Int. Ed.* **2006**, *45*, 285–290; *Angew. Chem.* **2006**, *118*, 291–296; c) A. Nguyen, S. Top, P. Pigeon, A. Vessières, E. A. Hillard, M. A. Plamont, M. Huché, C. Rigamonti, G. Jaouen, *Chem. Eur. J.* **2009**, *15*, 684–696; d) D. Hamels, P. M. Dansette, E. A. Hillard, S. Top, A. Vessières, P. Herson, G. Jaouen, D. Mansuy, *Angew. Chem. Int. Ed.* **2009**, *48*, 9124–9126; *Angew. Chem.* **2009**, *121*, 9288–9290; e) D. Plažuk, A. Vessières, E. A. Hillard, O. Buriez, E. Labbé, P. Pigeon, M.-A. Plamont, C. Amatore, J. Zakrzewski, G. Jaouen, *J. Med. Chem.* **2009**, *52*, 4964–4967.
- [34] B. Bildstein, M. Malaun, H. Kopacka, K. Wurst, K.-H. Ongania, G. Opromolla, P. Zanello, *Organometallics* **1999**, *18*, 4325–4336.
- [35] D. Kanamori, A. Furukawa, T. Okamura, H. Yamamoto, N. Ueyama, *Org. Biomol. Chem.* **2005**, *3*, 1453–1459.
- [36] N. G. Connelly, W. E. Geiger, *Chem. Rev.* **1996**, *96*, 877–910.
- [37] Y. Kondo, in: *Supperbases for Organic Synthesis* (Ed.: T. Ishikawa), Wiley, Chichester, UK, **2009**, p. 145–185.
- [38] R. Prins, *Mol. Phys.* **1970**, *19*, 603–620.
- [39] G. R. Eaton, S. S. Eaton, D. P. Barr, R. T. Weber, *Quantitative EPR*, Springer, Vienna/New York, **2010**.
- [40] B. S. Brunshwig, C. Creutz, N. Sutin, *Chem. Soc. Rev.* **2002**, *31*, 168–184.
- [41] a) D. Siebler, C. Förster, K. Heinze, *Eur. J. Inorg. Chem.* **2010**, 3986–3992; b) T. Tagg, H. G. Kjaergaard, J. R. Lane, C. J. McAdam, B. H. Robinson, J. Simpson, *Organometallics* **2015**, *34*, 2662–2666.
- [42] J. Disinger, S. E. Manahan, *Anal. Lett.* **1982**, *15*, 1017–1029.
- [43] P. M. Tolstoy, B. Koepppe, G. S. Denisov, H.-H. Limbach, *Angew. Chem. Int. Ed.* **2009**, *48*, 5745–5747; *Angew. Chem.* **2009**, *121*, 5855–5858.
- [44] R. J. LeSuer, C. Buttolph, W. E. Geiger, *J. Organomet. Chem.* **2004**, *76*, 6395–6041.
- [45] N. Camire, U. T. Mueller-Westerhoff, W. E. Geiger, *J. Organomet. Chem.* **2001**, *639*, 823–826.
- [46] W. L. Mock, D. C. Y. Chua, *J. Chem. Soc. Perkin Trans. 2* **1995**, 2069–2074.
- [47] S. Panagiota, M. Louloui, Y. Deligiannakis, *Chem. Phys. Lett.* **2009**, *472*, 85–89.
- [48] P. Neta, R. W. Fessenden, *J. Phys. Chem.* **1974**, *78*, 523–529.
- [49] L. W. Kiruri, L. Khachatryan, B. Dellinger, S. Lomnicki, *Environ. Sci. Technol.* **2014**, *48*, 2212–2217.
- [50] J. W. Whittaker, *Chem. Rev.* **2003**, *103*, 2347–2363.
- [51] F. Thomas, O. Jarjayes, H. Jamet, S. Hamman, E. Saint-Aman, C. Duboc, J.-L. Pierre, *Angew. Chem. Int. Ed.* **2004**, *43*, 594–597; *Angew. Chem.* **2004**, *116*, 604–607.
- [52] T. Maki, Y. Araki, Y. Ishida, *J. Am. Chem. Soc.* **2001**, *123*, 3371–3372.
- [53] S. Vanicek, H. Kopacka, K. Wurst, S. Vergeiner, L. Oehninger, I. Ott, B. Bildstein, *Z. Anorg. Allg. Chem.* **2015**, *641*, 1282–1292.
- [54] M. Breza, *J. Mol. Struct.* **2004**, *683*, 167–169.
- [55] P. Pelikán, L. Omelka, K. Brudíková, M. Breza, *J. Mol. Struct.* **2003**, *624*, 251–255.
- [56] L. Omelka, J. Kováčová, *Magn. Reson. Chem.* **1994**, *32*, 525–531.
- [57] S. Terabe, R. Konaka, *J. Chem. Soc. Perkin Trans. 2* **1972**, 2163–2172.
- [58] S. Stoll, A. Schweiger, *J. Magn. Reson.* **2006**, *178*, 42–55.
- [59] *SMART Data Collection Software for the SMART System*, various versions, Bruker Analytical X-ray Instruments, Inc., Madison, WI, **2000**; *SAINT-Plus Data Processing Software for the SMART System*, various versions, Bruker Analytical X-ray Instruments, Inc., Madison, WI, **2000**.
- [60] R. H. Blessing, *Acta Crystallogr., Sect. A* **1995**, *51*, 33–38.
- [61] G. M. Sheldrick, *SHELXTL*, version 5.1, Bruker AXS, Madison, WI, **1998**.
- [62] G. M. Sheldrick, *SHELXL-97*, University of Göttingen, Germany, **1997**.
- [63] F. Neese, *WIREs Comput. Mol. Sci.* **2012**, *2*, 73–78.
- [64] A. Schäfer, H. Horn, R. Ahlrichs, *J. Chem. Phys.* **1992**, *97*, 2571–2577.
- [65] F. Weigend, R. Ahlrichs, *Phys. Chem. Chem. Phys.* **2005**, *7*, 3297–3305.
- [66] F. Neese, *Chem. Phys. Lett.* **2000**, *325*, 93–98.
- [67] T. H. Fischer, J. Almlof, *J. Phys. Chem.* **1992**, *96*, 9768–9774.
- [68] E. van Lenthe, E. J. Baerends, J. G. Snijders, *J. Chem. Phys.* **1993**, *99*, 4597–4610.
- [69] C. van Wüllen, *J. Chem. Phys.* **1998**, *109*, 392.
- [70] D. A. Pantazis, X. Y. Chen, C. R. Landis, F. Neese, *J. Chem. Theory Comput.* **2008**, *4*, 908–919.
- [71] S. Sinnecker, A. Rajendran, A. Klamt, M. Diedenhofen, F. Neese, *J. Phys. Chem. A* **2006**, *110*, 2235–2245.

Received: December 22, 2015

Published Online: February 12, 2016